

**MATHEMATICAL MODELS  
FOR  
EVAPORATION OF  
THIN FILMS**

by

Vikramjit Singh Rathee

A thesis submitted to the Faculty of the University of Delaware in partial fulfillment of the requirements for the degree of Honors Bachelor of Sciences in Chemical Engineering with Distinction

2013

© 2013 Vikramjit Singh Rathee  
All Rights Reserved

**MATHEMATICAL MODELS**  
**FOR**  
**EVAPORATION OF**  
**THIN FILMS**

by

Vikramjit Singh Rathee

Approved: \_\_\_\_\_  
Dr. Richard J. Braun, Ph.D. in Applied Mathematics  
Professor in charge of thesis on behalf of the Advisory Committee

Approved: \_\_\_\_\_  
Dr. Prasad S. Dhurjati, Ph.D. in Chemical Engineering  
Committee member from the Department of Chemical Engineering

Approved: \_\_\_\_\_  
Dr. James L. Glancey, Ph.D. in Mechanical Engineering  
Committee member from the Board of Senior Thesis Readers

Approved: \_\_\_\_\_  
Michael Arnold, Ph.D.  
Director, University Honors Program

## **ACKNOWLEDGMENTS**

First and foremost I am grateful to God for being my strength and my guide in the completion of this thesis, providing me the energy and the ability to do so.

I wish to express my sincere and profound gratitude to my adviser Professor Richard Braun for his illuminating guidance, constant encouragement and forbearance in devoting much time to read my work over and over again. His constructive advice and insightful discussions paved way for successful completion of this thesis.

Thank you Michael Stapf for helping me in difficult situations and offering me timely help and friendly advice whenever required. I really appreciate your collaboration, support and efforts in working through chapter 4 of the thesis.

I am wholeheartedly indebted to my parents for their love, care, motivation and support all through the years. My mother has been a pillar of strength for me in times of distress and always encouraged me to march ahead with courage and confidence.

It gives me immense pleasure to record my gratitude to Babaji and Safi Mausi who very kindly and generously took out time to pray for me and inspired me to put in my best efforts with full determination. I thank them for their blessings all the time.

My sincere thanks to Meg Meiman and Emily Miller for patiently directing and guiding me through the various stages of this undergraduate research.

I will also like to place on record my sincere thanks to the UD Honors program and the University of Delaware for providing me the opportunity to work on this thesis.

## TABLE OF CONTENTS

LIST OF FIGURES .....	vi
ABSTRACT .....	viii
1 INTRODUCTION .....	1
1.1 Structure of the Tear Film .....	1
1.2 Thinning Rate of Tear Film .....	2
1.3 Thesis outline.....	4
2 EVAPORATION OF ULTRA-THIN FILMS.....	6
2.2 Numerical approximation.....	12
2.3 Evolution of film thickness .....	13
2.5 Steady state solution .....	18
3 MOVING BOUNDARY PROBLEM .....	20
3.1 Numerical approximation.....	22
3.2 Concentration profile across the domain as a function of time .....	24
3.3 Comparison with fixed boundary condition .....	27
4 EVAPORATION WITH FLUID MOTION INSIDE THE FILM .....	31
4.1 Lubrication model .....	32
4.1.1 Boundary conditions.....	34
4.1.2 Derivation of Lubrication equation .....	36
4.2 Expression for evaporation rate.....	37
5 CONCLUSIONS .....	46
REFERENCES .....	48
6 APPENDIX .....	50
6.1 Code used for numerical simulation (Ch-2 and Ch-3) .....	50



## LIST OF FIGURES

<b>Figure 1:</b> Three layer viewpoint of the tear film (Braun 2012) .....	1
<b>Figure 3:</b> Sketch of the configuration on which mathematical models for evaporation are based. $C(z, t)$ is the vapor concentration profile across the $z$ coordinate. ....	4
<b>Figure 4:</b> Schematic showing the domain of vapor diffusion, far field humidity and concentration profile along the $z$ -coordinate for diffusion. ....	7
<b>Figure 5:</b> Non-dimensional film thickness as a function of non-dimensional time. The blue line is the van der Waals model solution and the green line is the analytical solution <sup>[3]</sup> .....	13
<b>Figure 6:</b> Non-dimensional film thickness as a function of non-dimensional time. The blue line is the Polar model solution and the green line is the analytical solution .....	14
<b>Figure 9:</b> Plot of concentration of vapor at different $z$ values at $t = 5000$ . ....	19
<b>Figure 10:</b> Schematic showing the domain of vapor diffusion, $h(t) \leq z \leq L$ , far field humidity $C_H$ , and concentration profile $C(z, t)$ along the $z$ -coordinate. .	20
<b>Figure 11:</b> 3-D representation of the evolution of concentration profile with time across the domain $0 \leq \zeta \leq l$ . Domain length in terms of $z$ -coordinate is $L=20$ . End time for simulation was $t = 150$ . ....	24
<b>Figure 12:</b> Evolution of concentration profile across the domain $0 \leq \zeta \leq l$ with time. $L = 20$ . ....	25
<b>Figure 13:</b> Evolution of concentration profile across the domain $0 \leq \zeta \leq l$ with time. $L = 5$ . ....	26
<b>Figure 14:</b> Evolution of film thickness with time. Blue line depicts solution for fixed boundary condition. Green represents solution for moving air-water interface condition. Red line represents the analytical solution. ....	28
<b>Figure 15:</b> Comparison between concentration profile for fixed boundary condition and moving boundary condition across the domain at different time	

points.  $L = 20$ . Red line represents the fixed domain and blue line indicates the moving domain..... 29

**Figure 17:** Schematic showing the uneven air-film interface, film thickness  $h(x, t)$  as function of  $x$ -coordinate and time and evaporation rate at the film surface  $J(x, t)$ . ..... 31

**Figure 18:** The air is not saturated with vapor. Concentration of vapor is function of  $x, z$ , and  $t$ . ..... 37

## **ABSTRACT**

Evaporation is a major cause of thinning of tear film which can eventually cause damage to ocular surface. The aim of the presented research was to analyze some of the many facets of evaporation of the aqueous layer of the tear film through development of mathematical models. In chapter 2, using the assumption of negligible film thickness, no fluid motion and a flat air/film interface, the diffusion equation for the water vapor concentration was solved numerically on a fixed domain and solutions were analyzed. Theoretical steady state predictions were also matched with solution profiles obtained from numerical simulation. Later, in chapter 3, film thickness was not overlooked and decrease in film thickness due to evaporation changed the domain for the vapor diffusion with time. The partial differential equations describing the diffusion of water vapors were then solved numerically on this moving domain by introducing a new independent variable which mapped the moving domain into fixed domain. Comparison between solution for the fixed boundary and moving boundary problems revealed that the use negligible thickness assumption did not represent the behavior of the system as accurately as expected. Lastly, in chapter 4, a lubrication model was derived using a thin film approximation which related film thickness, evaporation rate and fluid motion. Further, expression for evaporation rate was developed for the deformed thin film where vapor diffusion outside the film limited the evaporation of liquid molecules. We hope to adapt this model of thin film dynamics to more complex tear film models in future research.

## INTRODUCTION

### 1.1 Structure of the Tear Film

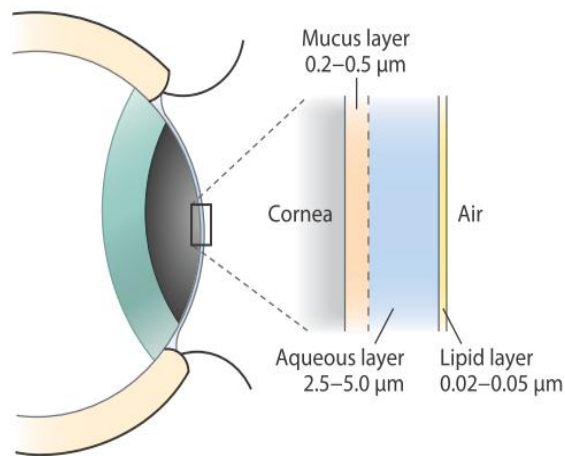


**Figure 1:** Three layer viewpoint of the tear film (Braun 2012)

Figure 1 is the sketch of the eye with the overlying tear film. The aqueous layer is essentially what is commonly thought of as tears. Tears are produced by lacrimal glands. The three layered tear film in humans plays an important role in maintaining the health and function of the eye<sup>[1]</sup>. The tear film provides not only a surface for strong refraction of light but also keeps the ocular surface moist and provides protection against dust and bacteria by transporting them away from the ocular surface<sup>[1]</sup>. The mucus layer (formed of mucins tethered to the corneal epithelium) is not a separate layer, but is rather part of the aqueous layer. The lipid

layer decreases the surface tension at the air-tear film interface, reducing thinning of the film due to evaporation and thus preventing tear film breakup in the eye <sup>[1]</sup>.

Dry eye syndrome (DES) is the problem associated when there is inadequate tear film on the ocular surface or from excessive evaporation of water from the tear film. Over 4.91 million Americans suffer from DES <sup>[1]</sup>, hence understanding tear film dynamics would help in further advancement in treatment for this syndrome.

## **1.2 Thinning Rate of Tear Film**

DES can be caused

(1) Due to deficient tear production by the lacrimal gland such that a complete tear film layer is not formed over the cornea <sup>[2]</sup>, or

(2) Due to rapid or prolonged evaporation of the tear film <sup>[2]</sup> i.e. adequate amount of tears are produced by the lacrimal glands but due to evaporation a complete layer of tear film is not formed over the ocular surface, also termed as evaporative dry eye syndrome.

Figure 2 depicts the movement of water in the tear film. There is sideways motion of the tear film present along with the evaporation of the water molecules from the tear film. The sideways motion of the tear film is due to tear film being constantly being drained into the tear duct to remove dust and bacteria from the ocular surface <sup>[1]</sup>. Chapter 2 and 3 deals with evaporative process of thin films under the assumption of insignificant fluid motion whereas evaporation with fluid motion is tackled in chapter 4.

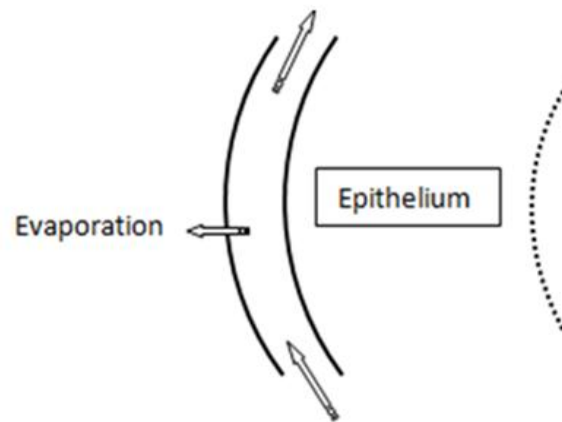


**Figure 2:** Thinning of tear film.

King-Smith et al. 2008 investigated the effect on evaporation rate of the tear film when using pre-ocular chambers/goggles<sup>[2]</sup>. Normal air flow over the corneal surface was prevented when using these goggles. It was concluded that evaporation is the major cause of thinning of tear film as thinning rate decreased substantially when using pre-ocular goggles as compared to rates in the presence of normal air flow (without goggles) because when using goggles a relatively thick humid layer developed over the corneal surface, hence the concentration gradient required for diffusion of water molecules from the tear film decreased and thus the evaporation rate decreased. This evidence also suggests that evaporation rate of the tear film is dependent upon the humidity of the atmosphere surrounding the eye.

The process of evaporation can be viewed as diffusion limited process or a mass transport limited process. The former involves use of Fick's law of diffusion and the standard diffusion equation with diffusion coefficient whereas the latter involves mass transfer correlations such as Sherwood number,  $Sh$  (ratio of convective transport to diffusive transport) and Schmidt number,  $Sc$  (ratio of viscous diffusion rate to

molecular diffusion rate). In the present research the evaporation was considered a diffusion limited process and hence mass transfer correlations were not used in development of evaporation models.

Figure 3 depicts a simplified sketch of the evaporation of the tear film used for the development of mathematical models. Lipid layer and surfactants (mucins) were not considered in development of these models.

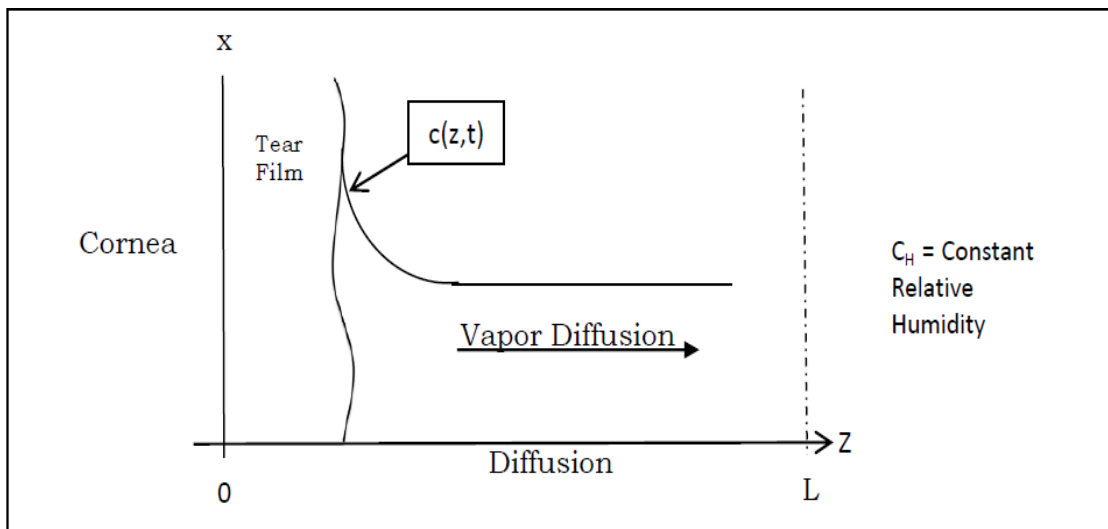


**Figure 3:** Sketch of the configuration on which mathematical models for evaporation are based.  $C(z, t)$  is the vapor concentration profile across the  $z$  coordinate.

### 1.3 Thesis outline

In chapter 2 work done by Ajaev et al. 2010 on fixed boundary problem (domain of diffusion fixed) was revisited<sup>[3]</sup>. Additional plots (2D and waterfall plots) depicting vapor concentration profile across the domain (outside the film) at different times are also presented in chapter 2.

In chapter 3, research was extended to moving boundary problem (domain of diffusion changing with time). New variable was introduced to scale the domain and a new set of partial differential equations with corresponding boundary conditions and initial conditions was developed and solved to produce plots of evolution of film thickness and vapor concentration profile at different times. Comparison between the fixed boundary problem and moving boundary problem in terms of concentration profile across the domain and evolution of film thickness and was also carried out in chapter 3.

In chapter 4, a lubrication model was derived using Navier-Stokes equation and boundary stresses which related the film thickness with fluid motion and evaporation rate. Navier-Stokes equation and boundary stresses were non-dimensionalised and lubrication theory (length of film  $\gg$  thickness of the film) was used to eliminate terms from these equations. Later, work done by Sultan et al 2004<sup>[4]</sup> was revisited. The objective was to approximate diffusion outside the film with the vapor concentration terms at the film surface. Further, equation for evaporation rate was derived which revealed that the equation provided by Sultan et al.<sup>[4]</sup> was missing terms and parameters, hence the newer version for the expression of evaporation rate has being provided in chapter 4.

## Chapter 2

### EVAPORATION OF ULTRA-THIN FILMS

Under isothermal conditions, water molecules from a uniform film will evaporate if the vapor pressure of the water in the gas phase above the film is below saturation pressure at that particular temperature. Due to evaporative flux, the film thickness would start decreasing. The process of evaporation occurs in order to achieve thermodynamic equilibrium when temperature and pressure is uniform throughout the system (liquid + vapor) and the vapor pressure is equal to saturation pressure<sup>[14]</sup>.

When a uniform thin film evaporates, the film thickness decreases to a value where surface forces become important and the exchange of molecules between two phases (liquid and air + vapor) equilibrates, evaporation stops and film thickness reaches an equilibrium value. This phenomenon is accounted for in mathematical models for evaporation by including an extra term known as the conjoining pressure, denoted here by  $\Pi$ . The conjoining pressure arises due to the different intermolecular interaction energies of liquid molecules with solid surface molecules and gas phase molecules. The conjoining pressure can be expressed as  $P = P_0 + \Pi$ , where  $P_0$  is the pressure of the bulk liquid and  $P$  is the pressure in thin film consisting of same liquid molecules as bulk liquid. For positive values of  $\Pi$ , evaporation is completely suppressed at a finite film thickness<sup>[14]</sup>.

The two main processes for vapor transport outside the film are diffusion and convective transport. To understand diffusion of vapor from the tear film into the air,

the tear film thickness was assumed to be independent of  $x$ -coordinate, have negligible fluid motion and negligible thickness compared to the domain outside the film. Hence, the domain of vapor diffusion was fixed,  $0 \leq z \leq L$  as shown in the figure 5 where  $L$  is the outer boundary of domain of diffusion. This case is called the “fixed boundary condition”. As the liquid evaporates, the film thickness decreases and the vapors diffuse in the  $z$ -direction towards a constant far field humidity. The low far-field concentration provides the necessary concentration gradient for diffusion at all times.

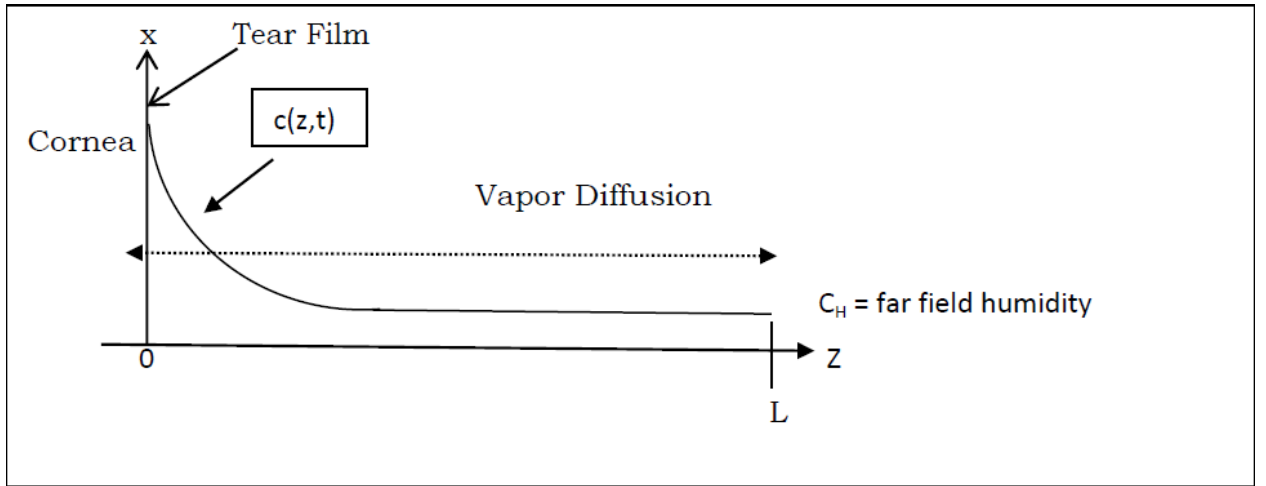


**Figure 4:** Schematic showing the domain of vapor diffusion, far field humidity and concentration profile along the  $z$ -coordinate for diffusion.

The importance of convective transport over diffusion is determined by Peclet number  $Pe = \frac{LV_g}{D}$ , where  $V_g$  is the characteristic speed of the gas phase.  $D$  is the diffusion coefficient of water vapor in the air at  $25^{\circ}C$ , which is  $\sim 10^{-6} m^2 s^{-1}$  (ref.18) and  $L$  is the length of the domain of diffusion. For  $Pe \ll 1$  convection of vapors can be neglected and using the values of  $D$  and  $L$ , the speed of the gas phase was estimated to be,  $V_g \ll 10^{-2} ms^{-1}$ . A speed of  $\sim 10^{-2} ms^{-1}$  is a reasonable value for the speed of the gas

phase at standard room temperature ( $25^{\circ}C$ ) and pressure ( $1 \text{ atm}$ ) in controlled environment such as a lab with no fans blowing. The effects of convection cannot be ignored in situations such as when riding a bike because the speed of the gas phase would be much higher and hence  $Pe$  would be too large. But, for development of mathematical models in this chapter and later chapters, such situations are not taken into consideration and hence, convective transport of water vapors was ignored.

Further, applying the condition of mass conservation at the film/air interface <sup>[14]</sup> i.e. mass lost due to evaporation is equal to diffusion flux,

$$\rho h_0 D L^{-2} \frac{\partial h}{\partial t} = D c_{sat} L^{-1} \frac{\partial c}{\partial z}$$

led to equation (2.2). Concentration profile across the domain is found by solving the diffusion equation (2.1). The constant far field concentration is  $C_H$ , (2.3). Thus, the equations governing the film evaporation are <sup>[3]</sup>:-

$$\frac{\partial C}{\partial t} = \frac{\partial^2 C}{\partial z^2} \tag{2.1}$$

$$\frac{\partial C}{\partial z}(0, t) = \frac{dh}{dt} \tag{2.2}$$

$$C(L, t) = C_H \tag{2.3}$$

To solve equation (2.1) – (2.3) and determine the unknowns  $C$  and  $h$ , two boundary conditions and two initial conditions are needed. One of the boundary condition is given as equation (2.3)

The scales are assumed as follows. For  $t$  it is  $(\rho h_0/c_{sat})^2 D^{-1}$ , the space variable  $z$  is  $\rho h_0/c_{sat}$ , variable  $c$  is  $c_{sat}$  <sup>[14]</sup>.  $c_{sat}$  is the saturation concentration,  $\rho$  is the density of the liquid and  $C(z, t)$  is the water vapor concentration in the air as a function of space coordinate  $z$  and time  $t$ .

## 2.1 Vapor concentration at the interface.

### 2.1.1 London van der Waals model of conjoining pressure

The condition for thermodynamic equilibrium requires not only that liquid and vapor phase be at same temperature and pressure but also that the chemical potential of both liquid and vapor phase is the same. The chemical potential or “escaping tendency” of the components of the two pure phases is same when there is no increase in the number of moles of the component in the liquid or vapor phase, i.e., there is no evaporation or condensation taking place at the vapor liquid interface. This can only happen at saturation conditions, therefore,

$$\mu_L^0(T_{sat}, P_v) = \mu_v^0(T_{sat}, P_v)$$

But, in thin films due to presence of conjoining pressure, the chemical potential of the liquid is modified; therefore, the new equilibrium condition would be

$$\mu_L - V_L \Pi = \mu_v$$

Where  $\mu_L$  and  $\mu_v$  are the chemical potential of the liquid in bulk and the vapor phase respectively.  $V_L$  is the molar volume of the liquid.

Since there is no appreciable change in number of liquid molecules in the process of acquiring thermodynamic equilibrium, hence assuming,  $\mu_L^0 = \mu_L$  and then

applying formula for variation in chemical potential of species in an ideal solution  $\mu_v = \mu_v^0 + RT \ln \left( \frac{c_{int}}{c_{sat}} \right)$ ,

$$c_{int} = c_{sat} e^{\frac{-V_L \Pi}{RT}}$$

(non-polar liquids) <sup>[14]</sup>

$$\Pi = -\frac{A}{h^3}$$

$C_0 = e^{-\check{\epsilon}/h_{eq}^3}$ , Where  $C_0 = \frac{c_{int}}{c_{sat}}$  is the new scaled equilibrium concentration of vapor at the interface and  $\check{\epsilon} = \frac{V_L |A|}{RT}$ . This also shows that concentration at the interface is a function of thickness in thin films hence  $C_0 = e^{-\check{\epsilon}/h^3}$  and  $A$  is the Hamaker constant (in Joules) represents the van der Waals interaction between molecules. Its value ranges from  $-10^{-19}$  to  $-10^{-20}$  Joules <sup>[15]</sup>. Here non-dimensional version of  $A$  is used in obtaining scaled vapour concentration at the interface. Film thickness  $h$  is scaled by  $h_0$ ,  $h_{eq}$  is the equilibrium film thickness and  $\check{\epsilon} = 10^{-3}$  (ref.3). Therefore, following is the set of equations to be tackled when this model is used.

$$\frac{\partial C}{\partial t} = \frac{\partial^2 C}{\partial z^2} \quad (2.4)$$

$$\frac{\partial C(0, t)}{\partial z} = \frac{dh}{dt} \quad (2.5)$$

BC's

$$C(L, t) = C_H \quad (2.6)$$

$$C(0, t) = C_0(t) = e^{-\check{\epsilon}/h^3} \quad (2.7)$$

IC's

$$C(0, 0) = C_0(0) = e^{-\check{\epsilon}/h_0^3} \quad (2.8)$$

$$C(z, 0) = C_H \text{ and } h_0 = h(0) = 1 \quad (2.9)$$

Where  $h$  is the film thickness at any time  $t$ ,  $h_0$  is the initial thickness of the thin film ( $t = 0$ ) and  $C_0(0)$  is the vapor concentration at the interface at  $t=0$ .

### 2.1.2 Polar model of conjoining pressure

Since molecules of polar liquids like water possess dipole moments, therefore a different model is used to represent conjoining pressure and concentration of vapor at the interface is modified as,

$$C(0, t) = C_0 = \exp(d_1 e^{-h/d_2}) \quad (2.10)$$

Hence the new set of equations is,

$$\frac{\partial C}{\partial t} = \frac{\partial^2 C}{\partial z^2} \quad (2.11)$$

$$\frac{\partial C(0, t)}{\partial z} = \frac{dh}{dt} \quad (2.12)$$

BC's

$$C(z = L, t) = C_H \quad (2.13)$$

$$C_0 = \exp(d_1 e^{-h/d_2}) \quad (2.14)$$

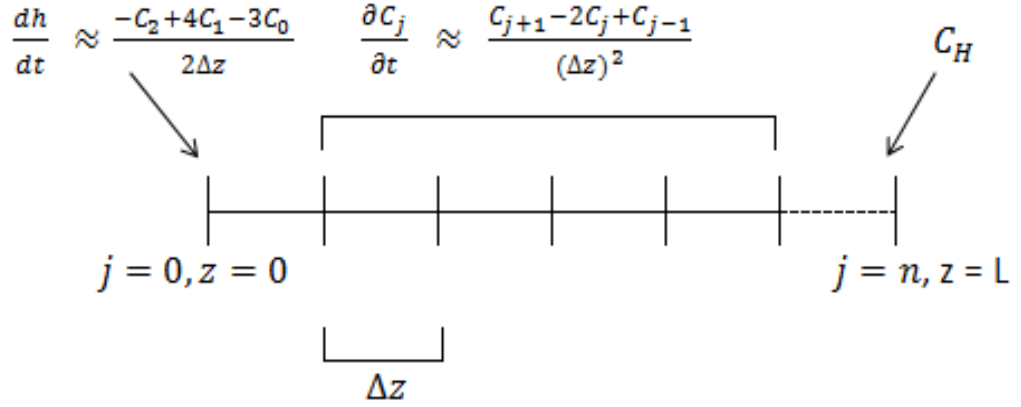
IC's

$$C(0,0) = C_0(0) = \exp(d_1 e^{-h_0/d_2}) \quad (2.15)$$

$$C(z, 0) = C_H \text{ and } h_0 = h(0) = 1 \quad (2.16)$$

## 2.2 Numerical approximation

System of equations (2.1) – (2.2) was solved using method of lines, discretizing the z-space with finite differences.



Where  $z_j = j\Delta z$ ;  $j$  is the grid point index and  $j = 0, 1, 2 \dots n$  and  $\Delta z$  is the spacing between grid points.  $n$  is the total number of grid points chosen.

Derivatives at  $z_j$  were approximated using the finite difference formulas; second-order forward difference formula to estimate  $\frac{\partial C}{\partial z}(0, t)$  and three-point centered difference formula for the second derivative  $\frac{\partial^2 C}{\partial z^2}$ .

$$\frac{\partial C}{\partial z}(0, t) \approx \frac{-C_2 + 4C_1 - 3C_0}{2\Delta z}$$

$$\frac{\partial^2 C_j(z_j, t)}{\partial z^2} \approx \frac{C_{j+1} - 2C_j + C_{j-1}}{(\Delta z)^2}$$

Hence equation (2.1) and (2.2) were approximate as equation (2.17) and (2.18) respectively,

$$\frac{\partial C_j(z_j, t)}{\partial t} \approx \frac{C_{j+1} - 2C_j + C_{j-1}}{(\Delta z)^2} \quad (2.17)$$

$$j = 2, 3, 4 \dots n-1$$

$$\frac{dh(t)}{dt} \approx \frac{-C_2 + 4C_1 - 3C_0}{2\Delta z} \quad (2.18)$$

$$j = 1$$

Equations (2.170 – (2.18) along with appropriate BC's and IC's corresponding to either van der Waals model or Polar model were solved in MATLAB using ODE 45 solver which employs Runge-Kutta method for approximation of solutions of ordinary differential equations. The error per step size is on the order of  $O(h^4)$ . To increase the accuracy of the solutions relative ( $10^{-5}$ ) and absolute tolerance ( $10^{-6}$ ) values were set such that if the error per step size exceeds the set tolerance values then the solver dynamically adjusts its step size (reduces step size) so that the error estimate remains below the set tolerances.

### 2.3 Evolution of film thickness

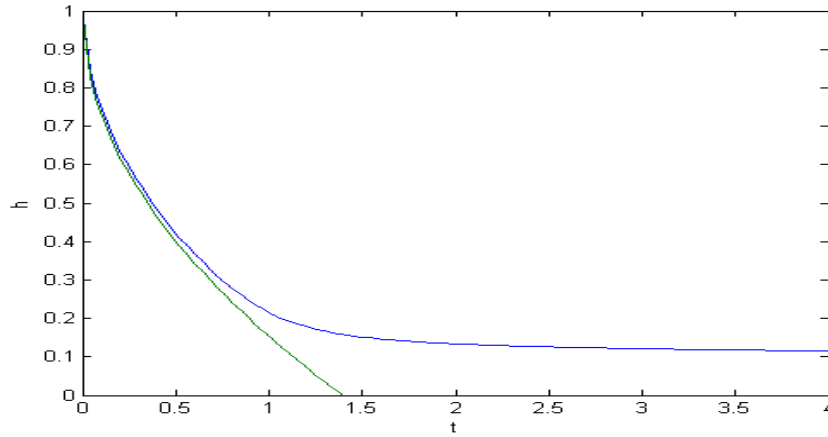


**Figure 5:** Non-dimensional film thickness as a function of non-dimensional time. The blue line is the van der Waals model solution and the green line is the analytical solution <sup>[3]</sup>.

In Figure 5, the blue line is the van der Waals model ( $c_0 = e^{-\tilde{\epsilon}/h^3}$ ) solution and  $\tilde{\epsilon} = 10^{-3}$ (ref.3). The green line is the analytical solution with negligible conjoining pressure i.e.  $\Pi = 0$ . Figure 5 indicates that mass of water leaves the film in the form of vapor and hence there is decrease in the thickness of the film. Initially, behavior of both van der Waals model solution and analytical solution is similar and there is rapid change in thickness but after  $t \sim 1$ , the analytical solution indicates that the liquid evaporates completely whereas film thickness reaches an equilibrium value when the van der Waals model of conjoining pressure is taken into account.

The expression for equilibrium thickness, defined by

$$(h_\infty = \left( -\epsilon / \log C_H \right)^{1/3})$$

which can be obtained by substituting  $C_H$  in place of  $C_0$  in the equation (2.7). The non-dimensional equilibrium thickness value is calculated to be  $h_\infty = 0.1184$  by substituting value of  $C_H = 0.2498$  for and  $\tilde{\epsilon} = 10^{-3}$  (ref.3).

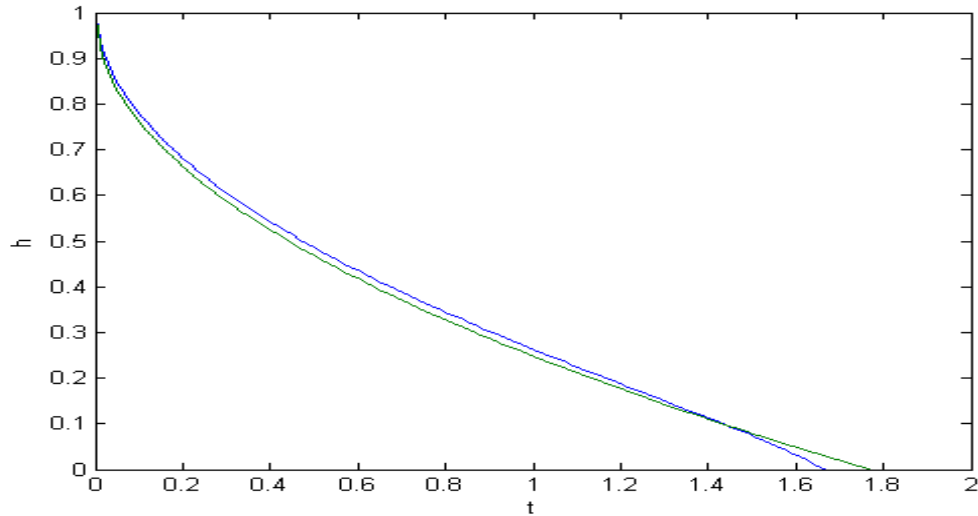


**Figure 6:** Non-dimensional film thickness as a function of non-dimensional time. The blue line is the Polar model solution and the green line is the analytical solution

In Figure 6, the blue line is the Polar model ( $c_0 = \exp(d_1 e^{-h/d_2})$ ) solution where  $d_1 = d_2 = 0.1$  [3] and the green line is the analytical solution with negligible disjoining pressure i.e.  $\Pi = 0$ . The solutions of Polar model of conjoining pressure and analytical solution ( $\Pi = 0$ ) indicate that film thickness goes down to zero (thin film evaporates completely) as can be analyzed from the Figure 6. Therefore, polar liquids such as water would evaporate completely instead of approaching a non-zero equilibrium thickness value.

Figure 7 suggests that if aqueous layer is primarily composed of water then the tear film should evaporate completely after sometime, but this is not the case due to presence of mucins in the tear film. Some mucins are untethered and floating around in the aqueous layer and some are tethered at the corneal epithelial cell surface.

The highly-glycosylated mucins present in the aqueous layer of the tear film are hydrophilic and thus they help in wetting of the cornea by maintaining adequate water content in the tear film [1], [12], and [13], apart from that, with each blink tear film is reformed thus the tear film thickness essentially never goes down to zero. Hence, the London-van-der Waals model would be much more useful in modeling tear films because the thin film doesn't completely evaporate and the film thickness never goes down to zero (figure 5), therefore usage of London-van-der Waals model would give better approximation for the evaporation of the tear film of the eye. Where as in case of Polar model, the film evaporates completely and film thickness goes down to zero (figure 6).

## 2.4 Time dependent concentration profile across the domain

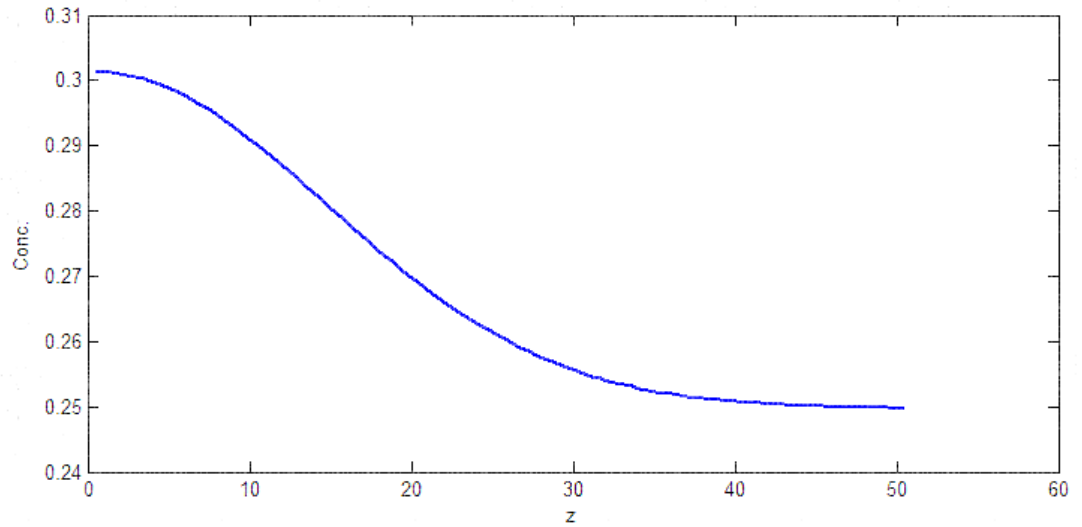


**Figure 7:** Plot of concentration of vapor at different  $z$  values at  $t = 100$ .

Figure 7 shows that during early times of the evaporation process, concentration gradient is present for diffusion of water vapor into the air, with concentration of vapors higher near the interface and a fixed constant value of  $C_H$  ( $\sim 0.25$ ) at the far field. The constant far field concentration acts as a desiccant and maintains concentration gradient for diffusion to occur.

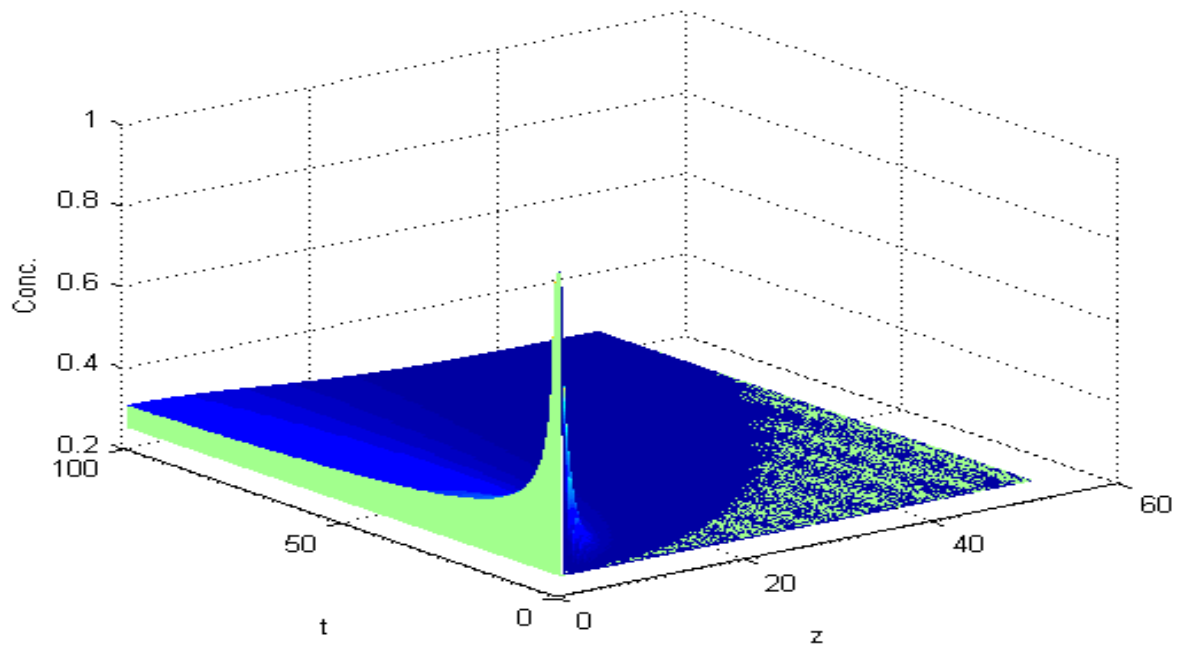


**Figure 8:** Waterfall plot for concentration profile across the domain. End time for simulation was  $t = 100$

In figure 8, the peak at  $z = 0$  and  $t = 0$  indicates high concentration of vapors near the interface at  $z = h$ . Also, at  $t = 0$ , concentration profile is relatively flat at most  $z$  values but at higher times there is bump in the concentration profile (blue) at higher  $z$  values such as  $z = 20$  indicating that some water vapor have diffused to position  $z = 20$ . At  $t = 100$  concentration profile starts to flatten out. Figure 8 also indicates that concentration at the interface decreases with time. Figure 7 corresponds to concentration of vapors at different  $z$  values at  $t = 100$  which would similar to taking cross section of the above plot at  $t = 100$ .

## 2.5 Steady state solution

According to Fick's second law (Non-steady state Diffusion)

$$\frac{\partial c}{\partial t} = D \frac{\partial^2 c}{\partial z^2} \quad (2.19)$$

where D is the diffusion coefficient

Under steady state conditions, concentration of vapor is same at all  $z$  values and equal to  $C_H$  i.e. there is no concentration gradient present for diffusion. Hence,

$$\frac{\partial^2 c}{\partial z^2} = 0 \text{ and } \frac{\partial c}{\partial t} = 0 \quad (2.20)$$

Integrating  $\frac{\partial^2 c}{\partial z^2} = 0$  leads to following relationship:

$$C(z) = \frac{C_H - C(0, t \rightarrow \infty)}{L} z + C(0, t \rightarrow \infty) \quad (2.21)$$

Diffusion is suppressed when concentration at the interface is equal to far field concentration i.e.  $C(0, t \rightarrow \infty) = C_H$ . Therefore,

$$C(z) = C_H$$

Since  $C_H = 0.2498$ , thus theoretically, at steady state, concentration of the vapor across the domain should be same and equal to relative humidity of the air,

$$C(z) = 0.2498$$

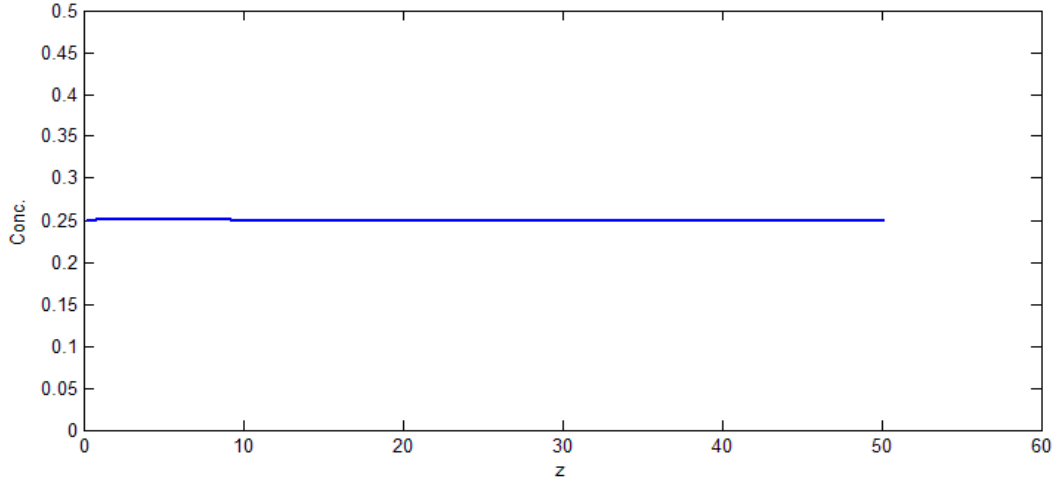


**Figure 9:** Plot of concentration of vapor at different  $z$  values at  $t = 5000$ .

The simulation results (figure 9) confirms the theoretical predication that at steady state  $C(z) \cong C_H = 0.2498$  i.e. the concentration at each grid point is equal to far field concentration. Gradient for diffusion is no longer present. Again, referring to figure 5, the film thickness has reached an equilibrium value much earlier. Therefore, the mass of water that had evaporated from the film is diffusing to larger  $z$  values at later times. Due to presence of constant far field concentration condition (desiccant) equilibrium concentration is reached at all  $z$  values eventually. A desiccant sustains a particular state of dryness and in the present case, constant field condition is maintaining relative humidity of  $C_H = 0.2498$  at  $z = L$ , hence the analogy of  $C_H$  to desiccant. This agreement between theoretical results and simulation results indicate that the equations (2.11) – (2.12) along with boundary conditions (2.13) – (2.14) and initial conditions (2.15) – (2.16) model the diffusion of vapor well.

## Chapter 3

### MOVING BOUNDARY PROBLEM

In chapter 2, evaporation of film was simplified by assuming that thickness of the film was very small and hence was neglected, therefore, the domain of diffusion was fixed to be  $0 \leq z \leq L$ .

Now, the assumption of negligible thickness is relaxed and hence the domain of diffusion is not fixed. The downward movement of air-water interface (decrease in film thickness) due to evaporation of water molecules changes the domain of diffusion with time therefore the domain of diffusion becomes  $h(t) \leq z \leq L$ , where  $h(t)$  is the film thickness as a function of time.  $h_{eq}$  is the equilibrium thickness of the film.

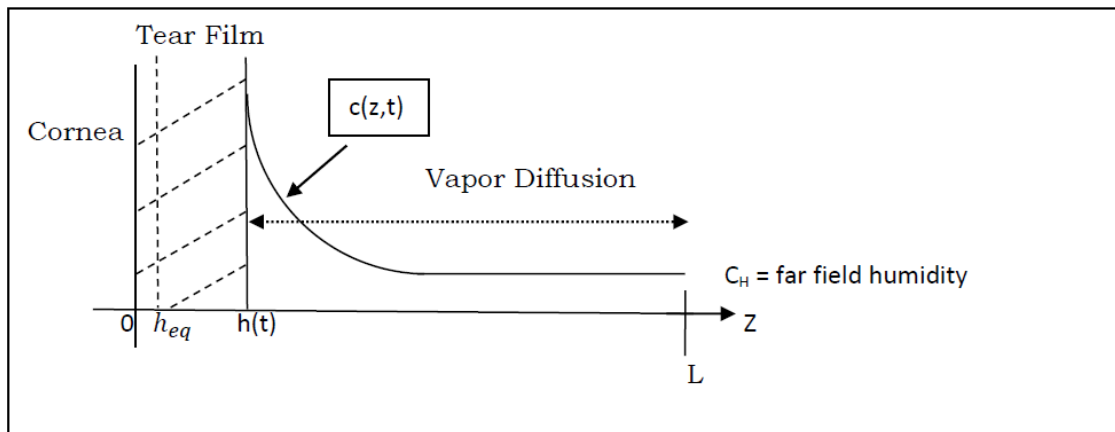


**Figure 10:** Schematic showing the domain of vapor diffusion,  $h(t) \leq z \leq L$ , far field humidity  $C_H$ , and concentration profile  $C(z, t)$  along the z-coordinate.

To simplify the problem of moving domain of diffusion, a new variable,  $\zeta$  was defined such that the domain becomes fixed again i.e.  $0 \leq \zeta \leq 1$ . Therefore, concentration of vapor becomes a function of  $\zeta$  and  $t$  (3.2), instead of  $z$  and  $t$ .

$$\zeta(t) = \frac{z - h(t)}{L - h(t)} \quad (3.1)$$

$$C(z, t) = \tilde{C}(\zeta, t) \quad (3.2)$$

Incorporation of equality presented in (3.2), equation (2.1) – (2.2) were modified to (3.3) – (3.4) and using London van der Waals model of conjoining pressure BC's (2.13) – (2.14) and IC's (2.15) – (2.16) were modified to (3.5) – (3.6) and (3.7) – (3.8) respectively. Equation (3.4) is valid at  $\zeta = 0$  i.e. the interface of the film. Thus, the equations governing the evolution of film thickness becomes,

PDE's

$$\frac{\partial \tilde{C}}{\partial t} = \frac{1}{(L - h)^2} \frac{\partial^2 \tilde{C}}{\partial \zeta^2} - \frac{(\zeta - 1)}{(L - h)} \frac{\partial \tilde{C}}{\partial \zeta} \cdot \frac{dh}{dt} \quad (3.3)$$

$$\frac{\partial \tilde{C}}{\partial \zeta}(0, t) = (L - h) \frac{dh}{dt} \quad (3.4)$$

Highlighted terms in (3.3) – (3.4) are the additional terms, got after modifying equation (2.1) – (2.2) through chain rule (since  $\zeta(t)$ ).

BC's

$$\tilde{C}(1, t) = C_H \quad (3.5)$$

$$\tilde{C}(0, t) = \tilde{C}_0 = e^{-\xi/h^3} \quad (3.6)$$

IC's

$$\tilde{C}(0,0) = \tilde{C}_0(0) = e^{-\xi/h_0^3} \quad (3.7)$$

$$\begin{aligned} \tilde{C}(\zeta, 0) &= C_H \\ \text{and } h_0 &= h(0) = 1 \end{aligned} \quad (3.8)$$

### 3.1 Numerical approximation

Again, the system of equation (3.3) – (3.4) was solved using method of lines, discretizing the  $z$ -space with finite differences. In this case,  $\zeta_j = j\Delta z$ ,  $j$  is the grid point index and  $j = 0, 1, 2 \dots n$  and  $\Delta z$  is the spacing between grid points.  $n$  is the total number of grid points chosen.

Derivatives at  $z_j$  were approximated using the second-order forward difference formula to estimate  $\frac{\partial \tilde{C}(0,t)}{\partial \zeta}$ , centered difference formula to approximate  $\frac{\partial \tilde{C}}{\partial \zeta}$  and three-

point centered difference formula for the second derivative  $\frac{\partial^2 \tilde{C}}{\partial \zeta^2}$ . Hence equation (3.3)

and (3.4) were approximate as equation (3.9) and (3.10) respectively,

$$\frac{\partial \tilde{C}_j}{\partial t} = \frac{1}{(L-h)^2} \left[ \frac{\tilde{C}_{j+1} - 2\tilde{C}_j + \tilde{C}_{j-1}}{(\Delta z)^2} \right] - \left( \frac{\tilde{C}_{j+1} - \tilde{C}_{j-1}}{2\Delta z} \right) \frac{(\zeta_j - 1)}{(L-h)^2} \left[ \frac{-\tilde{C}_2 + 4\tilde{C}_1 - 3\tilde{C}_0}{2\Delta z} \right] \quad (3.9)$$

$$j = 1, 2, 3 \dots n-2$$

$$\frac{dh}{dt} = \frac{1}{(L-h)} \left[ \frac{-\tilde{C}_2 + 4\tilde{C}_1 - 3\tilde{C}_0}{2\Delta z} \right] \quad (3.10)$$

$$j = 0$$

Also, the  $\frac{dh}{dt}$  term in equation (3.3) was replaced with equation (3.10) so that the equation (3.9) becomes an explicit ODE instead of implicit ODE.

At  $t = 0$ , the derivative at the air/film interface ( $\zeta = 0$ ) gives bad results because of the sudden jump in the IC from  $\tilde{C}(0,0) = \tilde{C}_0(0)$  to  $\tilde{C}(\zeta, 0) = C_H$ , hence, in order to smooth out the transition from  $\tilde{C}_0$  to  $C_H$  at  $t = 0$ , the IC at all the grid points in the domain except  $\zeta = 0$  i.e. equation (3.8) was modified as,

$$\tilde{C}(\zeta \neq 0,0) = (\tilde{C}_0(0) - C_H)e^{\frac{-j\Delta z}{0.05}} + C_H \quad (3.11)$$

Equation (3.9) – (3.10) along with equation (3.5) – (3.8) and (3.11) were solved in MATLAB using ODE 45.

### 3.2 Concentration profile across the domain as a function of time

The concentration gradient drives the diffusion of water vapor from lower  $\zeta$  values to higher  $\zeta$  values. Thus, at  $t = 150$ , concentration of the vapor at the interface has reached a value of  $\sim 0.35$  as compared to value of 1 at  $t = 0$ . This is represented by the peak, i.e. steep concentration gradient is not present at  $t = 150$  as it was present during earlier times. The constant concentration value of  $C_H = 0.2498$  at  $\zeta = 1$  acts as desiccant, therefore maintaining the concentration gradient for diffusion to occur. Cross-sections of the figure 11 at different time points would yield curves similar to presented in figure 12 for  $L = 20$ .

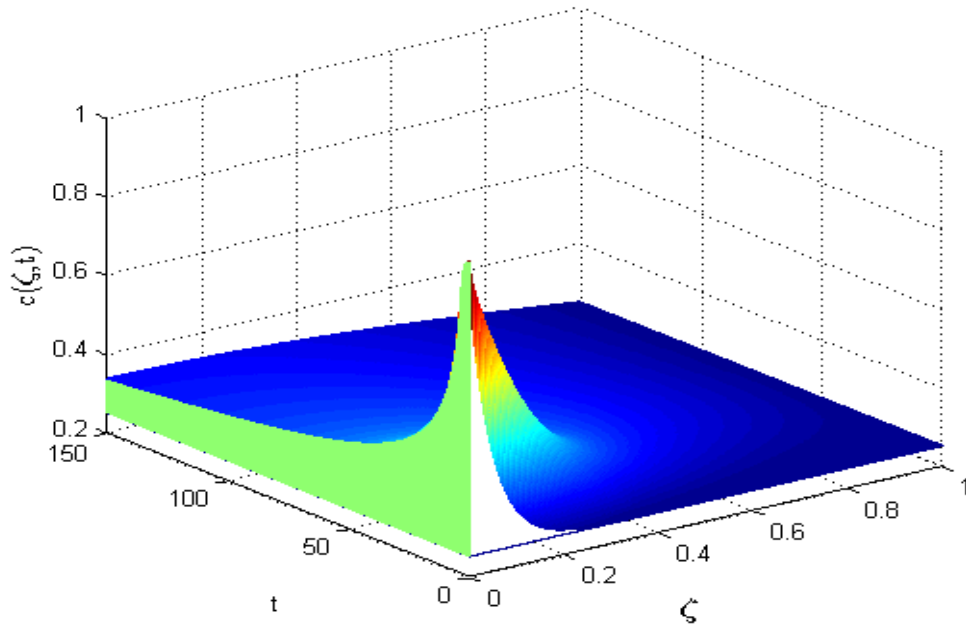


**Figure 11:** 3-D representation of the evolution of concentration profile with time across the domain  $0 \leq \zeta \leq 1$ . Domain length in terms of  $z$ -coordinate is  $L=20$ . End time for simulation was  $t = 150$ .

Both figures 12 and 13 depict the concentration of vapor as a function of  $\zeta$  that decrease with increase in time. This indicates the diffusion of vapor to larger  $\zeta$ 's and eventually concentration profile starts to even out. Also, analyzing figure 12 and 13, it can be inferred that equilibrium concentration across all  $\zeta$  is achieved faster when  $L = 5$ . This is because when domain is small, the constant far field humidity  $C_H$  condition (acting like a desiccant) is much closer to the film, and thus a larger high concentration gradient is maintained at early times. Since rate of diffusion is proportional to concentration gradient, the rate of diffusion is faster when  $L = 5$ , hence equilibrium concentration at all  $\zeta$  values is approached faster.

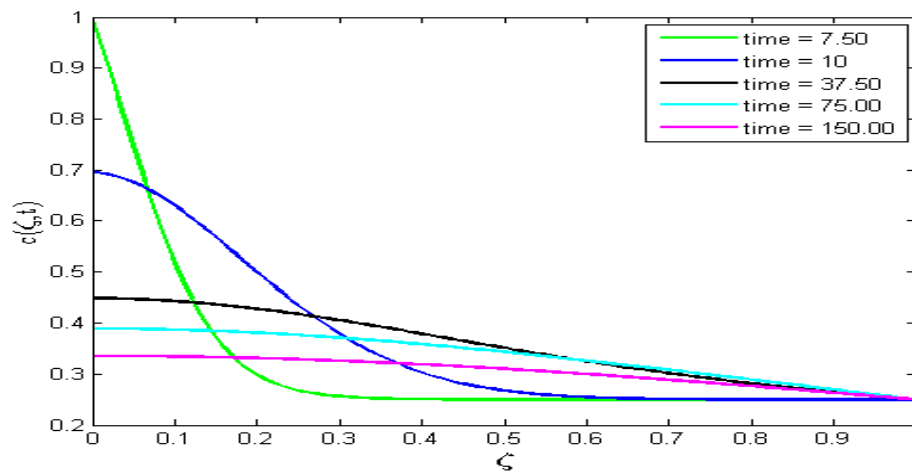


**Figure 12:** Evolution of concentration profile across the domain  $0 \leq \zeta \leq 1$  with time.  
 $L = 20$ .

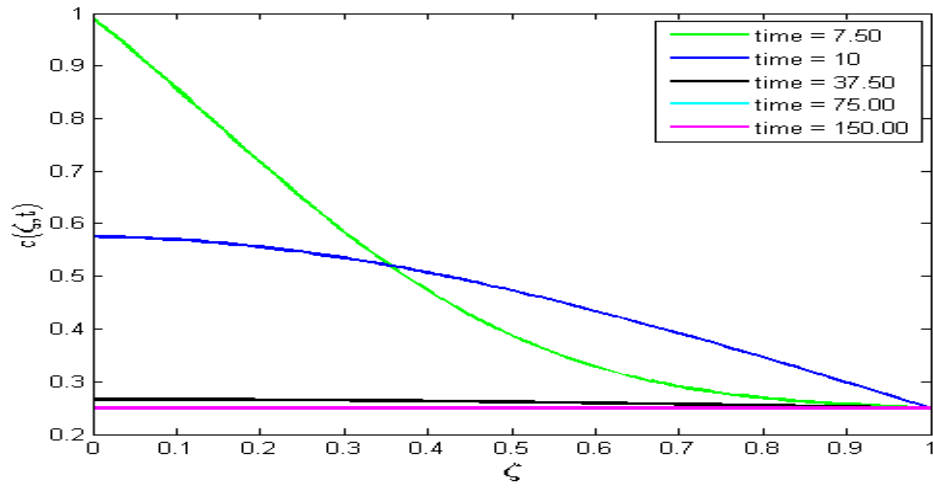


**Figure 13:** Evolution of concentration profile across the domain  $0 \leq \zeta \leq 1$  with time.  
 $L = 5$ .

### 3.3 Comparison with fixed boundary condition

In figure 14, the blue line is the solution for fixed boundary condition (diffusion domain  $0 \leq z \leq L$ ). The green line depicts solution for moving air-water interface condition ( $h(t) \leq z \leq L$ ). Red line is the analytical solution. For both fixed boundary condition and moving boundary condition van der Waals model of conjoining pressure was used ( $\tilde{C}_0 = e^{-\tilde{\epsilon}/h^3}$ ). Figure 14 indicates that with the assumption of negligible thickness, the air-water interface goes down faster and the film thickness approaches equilibrium value earlier as compared moving boundary condition. Solutions are very close at later times since in both conditions same equilibrium thickness value is achieved. The solutions are different initially hence the incorporation of moving interface and corresponding development of modified PDE's would give accurate depiction of the evolution of film thickness since one of the assumptions of negligible thickness is no longer valid. The analytical solution does not take into account conjoining pressure hence an equilibrium thickness value is not observed and the film completely evaporates.

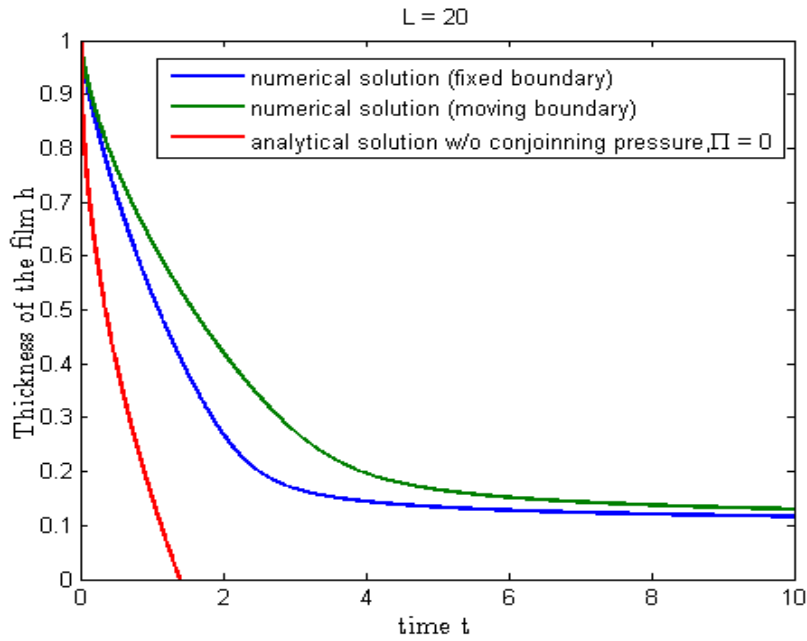


**Figure 14:** Evolution of film thickness with time. Blue line depicts solution for fixed boundary condition. Green represents solution for moving air-water interface condition. Red line represents the analytical solution.

In figure 15, initially ( $t = 0$  and  $t = 1$ ) the concentration profile doesn't seem to be different for either fixed boundary or moving boundary case as concentration profile for the moving boundary case just seem to be shifted to the right by the amount equal to the thickness of the film. The difference in profiles are observed after the film reaches equilibrium thickness of  $h_{eq} = 0.1184$  i.e. after  $t = 7.50$ . For  $t = 7.50$  and  $t = 37.50$ , the vapor hasn't quite reached towards the end of the domain (e.g.  $z = 19$ ) in both cases, but the  $z$  values to which vapor has diffused the concentration is higher in the case of moving boundary as compared to fixed boundary. The vapor has diffused to the end of the domain for  $t = 75$  and  $t = 150$  and again concentration of the vapor is

higher at each  $z$  coordinate for the moving boundary condition though the difference between concentration at each  $z$  value seems to be decreasing with time.

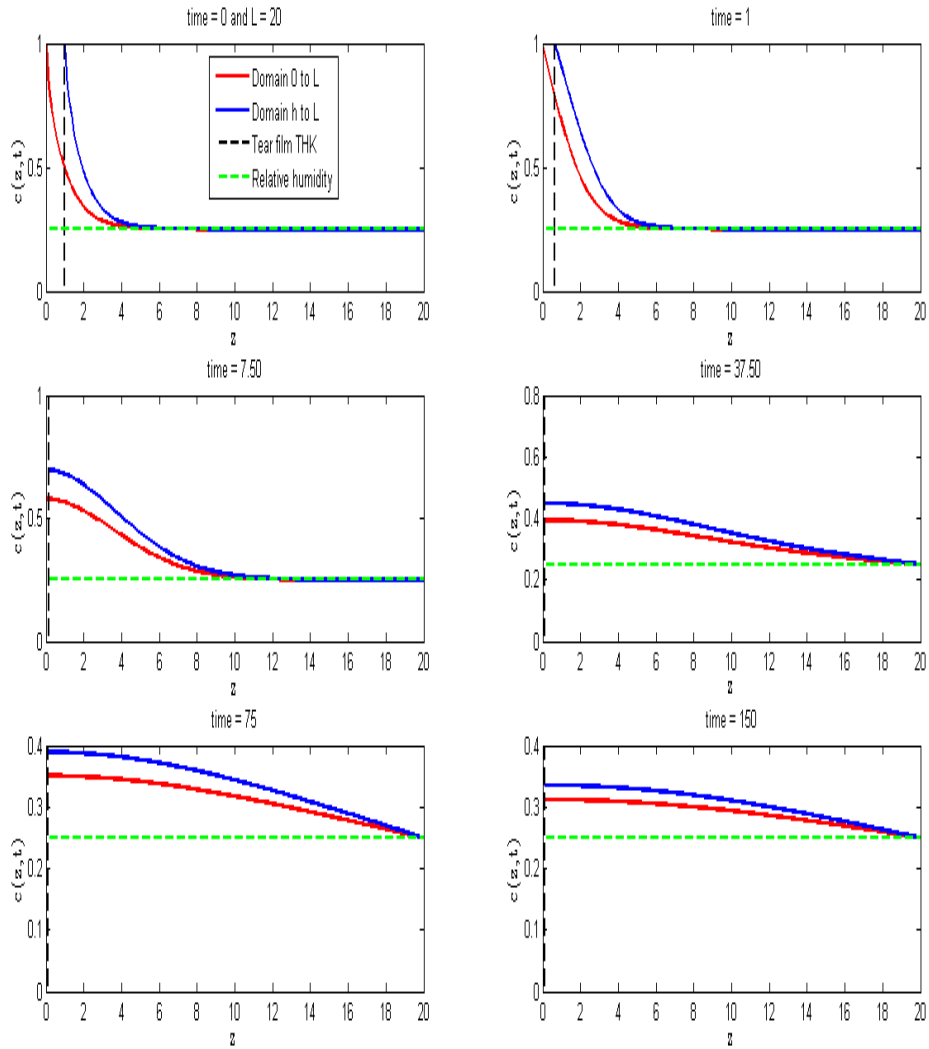


**Figure 15:** Comparison between concentration profile for fixed boundary condition and moving boundary condition across the domain at different time points.  $L = 20$ . Red line represents the fixed domain and blue line indicates the moving domain.

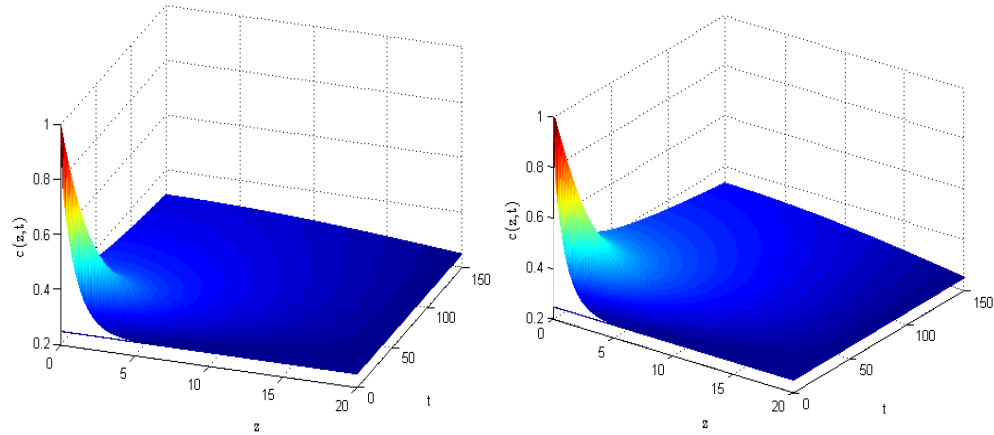


**Figure 16:** Fixed boundary,  $t = 150$ ,  $L = 20$

Moving boundary,  $t = 150$ ,  $L = 20$

Analyzing figure 14, for the fixed boundary problem, the rate of decrease in film thickness is faster for the fixed boundary problem as compared to the moving boundary problem. Also, from figure 16, the slope  $\frac{\partial C}{\partial z}(0, t)$  is steeper in case of fixed boundary problem as compared to the moving boundary problem. These results are in good agreement with the mass conservation condition at the interface,  $\frac{\partial C}{\partial z}(0, t) = \frac{dh}{dt}$  indicating that solution for both fixed boundary problem and moving boundary problem are indeed correct. Also, these results suggest that diffusion field has extended further into the domain in case of moving boundary problem as compared to fixed boundary problem, hence higher vapor concentration at all  $z$  values within the diffusion field for the moving boundary problem. This is in agreement with the results presented in figure 15.

### EVAPORATION WITH FLUID MOTION INSIDE THE FILM

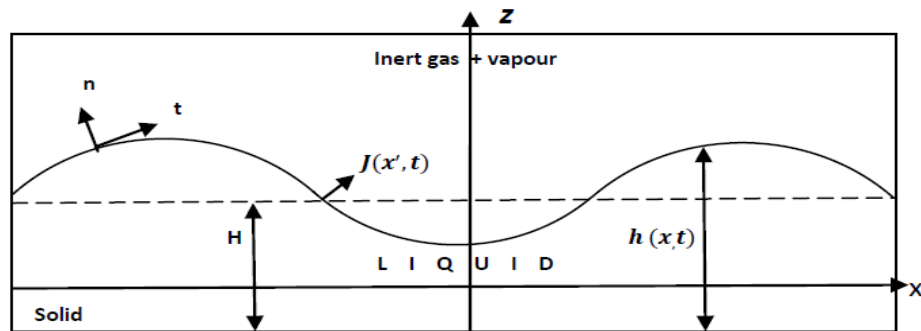


**Figure 17:** Schematic showing the uneven air-film interface, film thickness  $h(x, t)$  as function of  $x$ -coordinate and time and evaporation rate at the film surface  $J(x, t)$ .

In previous chapters, mathematical models were developed based on the assumption that the thin film was flat and there was negligible fluid motion present. This chapter deals in development of models for the evaporation of Newtonian fluid thin film; when fluid motion is present as well as when deflection from the flat plane (air-water interface) is weak, i.e. small wrinkles are present in the thin film. The tear film interface is not flat, therefore incorporation of wrinkled air-water interface in the model provides better resemblance to real thin films. Research work done by Sultan et al. 2004<sup>[4]</sup> was consulted for this section (4.2).

In section (4.1) we set out to derive lubrication model which related film thickness with fluid motion and evaporation rate. Due to presence of fluid motion the derivation was carried out using the principles of fluid dynamics. Lubrication theory

was used to eliminate terms from the non-dimensionalised Navier-Stokes equations, boundary stresses and kinematic equation and eventually lubrication model was derived.

Since lubrication model includes a term for evaporation rate, hence exercise of deriving the analytical expression of evaporation rate was carried out in section (4.2). For this purpose research work done by Sultan et al. 2004 was revisited. They wanted to study the stability of an evaporating thin film i.e. when evaporation induced flow in the film causing the wrinkles on the air-water interface <sup>[4]</sup>. With a series of approximation, external diffusion field was reduced to vapor concentration terms at the air-water interface. Eventually a single equation relating evaporation rate to film thickness was obtained which could then be substituted in the lubrication model for evaporation rate. In the present research we are revisiting Sultan et al. 2004 work and are correcting it and explaining it.

#### 4.1 Lubrication model

The motivation for deriving this model was to have an equation that related evaporation rate with film thickness and fluid motion.

For a Newtonian fluid, the  $x$ -momentum and  $y$ -momentum Navier-Stokes equations are given by (4.1) and (4.2) respectively.

$$\rho \left( \frac{\partial u'}{\partial t'} + \frac{\partial^2 u'}{\partial x'^2} + v' \frac{\partial u'}{\partial y'} \right) = \mu \left( \frac{\partial^2 u'}{\partial x'^2} + \frac{\partial^2 u'}{\partial y'^2} \right) - \frac{\partial p'}{\partial x'} \quad (4.1)$$

$$\rho \left( \frac{\partial v'}{\partial t'} + u' \frac{\partial v'}{\partial x'} + v' \frac{\partial^2 v'}{\partial y'^2} \right) = \mu \left( \frac{\partial^2 v'}{\partial x'^2} + \frac{\partial^2 v'}{\partial y'^2} \right) - \frac{\partial p'}{\partial y'} \quad (4.2)$$

Non-dimensionalization of Equations (4.1) and (4.2) along with non-dimensionalization of other equations later in this section is carried out by using the following scales:

$$\begin{aligned} x' &= L_x x, & y' &= L_y y, & u' &= Uu, & v' &= Vv, & p' &= Pp, \\ t' &= \frac{L_x}{V} t, & h' &= \varepsilon L_x h, & \varepsilon &= \frac{L_y}{L_x} \end{aligned}$$

Where variables without superscript(') are the non-dimensionalised variables. For thin films, thickness of the film is much smaller as compared to the length of the film, therefore,  $\frac{L_y}{L_x} = \varepsilon$ , and  $\varepsilon \ll 1$ . Hence, after non-dimensionalization of (4.1) and (4.2), all the terms with coefficients on the order of  $\varepsilon$  were eliminated resulting in equation (4.3) and (4.4) respectively.

Additionally, using the incompressibility assumption (density is constant), the continuity equation (conservation of mass),

$$\frac{\partial \rho}{\partial t} + \nabla \cdot \rho \vec{u}' = 0$$

is reduced to,

$$\nabla \cdot \vec{u}' = 0$$

non-dimensionalization of which, gave equation (4.5).

$$u_{yy} = p_x \tag{4.3}$$

$$p_y = 0 \tag{4.4}$$

$$u_x + v_y = 0 \tag{4.5}$$

Here,  $u$  is the  $x$ -component and  $v$  is the  $y$ -component of the velocity of the fluid.

### 4.1.1 Boundary conditions

There are two types of stresses acting at the air-water interface,  $y' = h'(x', t')$ ; Normal boundary stress (4.6) and tangential stress (4.7). Since it is assumed there is no air flow outside the film hence, tangential stress is equal to 0.

$$\hat{n}^T \cdot T \cdot \hat{n} = -\sigma K \quad (4.6)$$

$$\hat{t}^T \cdot T \cdot \hat{n} = 0 \quad (4.7)$$

Where,

$$\hat{n} = \frac{1}{\sqrt{1+h_x^2}} \begin{pmatrix} -h_x \\ 1 \end{pmatrix} \text{ and } \hat{t} = \frac{1}{\sqrt{1+h_x^2}} \begin{pmatrix} 1 \\ h_x \end{pmatrix} \quad (4.8)$$

is obtained from the mathematical definition of unit normal vector and unit tangential vector respectively.

$T$  is the stress tensor and  $K$  is the curvature of the interface

$$T = \mu \begin{pmatrix} 2u_x & u_y + v_x \\ u_y + v_x & 2v_y \end{pmatrix} - \begin{pmatrix} p & 0 \\ 0 & p \end{pmatrix}. \quad (4.9)$$

$$K = \frac{h_{xx}}{(1+h_x^2)^{3/2}} \quad (4.10)$$

The curvature of the interface  $K$  represents how fast the curve changes direction at a given point, therefore, curvature of the interface can be found at a particular  $x$ -value and time by evaluating  $K$  at that particular value of  $x$  and  $t$ .  $\sigma$  represents surface

tension of the air/film interface and the product  $\sigma K$  is the pressure due to surface tension or “capillarity”.

Both equations (4.6) and (4.7) were non-dimensionalised to give (4.11) and (4.12) respectively.

$$p = -Sh_{xx}, \quad S = \frac{\sigma \epsilon}{P L_x} \quad (4.11)$$

$$u_y = 0 \quad (4.12)$$

Moreover, Kinematic equation (4.13) represents the mass balance at the air-water interface.

$$J' = \rho (\vec{V}_f - \vec{V}_i) \cdot \hat{n} \quad (4.13)$$

Where,

$$\vec{V}_f = \begin{pmatrix} u \\ v \end{pmatrix} \text{ and } \vec{V}_i = \begin{pmatrix} 0 \\ h_t \end{pmatrix} \quad (4.14)$$

$J'$  is the evaporative flux,  $\rho$  is the density of the water,  $\vec{V}_f$  is the velocity of the fluid and  $\vec{V}_i$  is the velocity of the interface.

Non-dimensionalization of (4.13) with scale for  $J'$  being  $J' = V\rho J$ , gives,

$$h_t - h_x u - v = -J \quad (4.15)$$

$V$  is the scale for the  $y$  component of the velocity ( $v$ )

Hence at  $y = h$ ,

$$\begin{aligned} p &= -Sh_{xx} \\ u_y &= 0 \end{aligned} \quad (4.16)$$

$$h_t - h_x u - v = -J$$

At  $y = 0$ , from no slip assumption,

$$u = v = 0 \quad (4.17)$$

#### 4.1.2 Derivation of Lubrication equation

From equation (4.4),  $p$  is a function only of  $x$  and  $t$  in the liquid, hence  $p = -Sh_{xx}$  holds throughout the liquid. Therefore, equation (4.11) was differentiated wr.t to  $x$  and equation (4.3) was integrated twice which led to (4.18).

$$u = -Sh_{xxx} \left( \frac{1}{2}y^2 - hy \right) \quad (4.18)$$

Further solving equation (4.5) and substituting for  $h_x u - v$  terms in the Kinematic equation (4.15), Lubrication equation (4.19) was found which relates film thickness with fluid motion with evaporation rate.

$$h_t + J + \frac{\partial}{\partial x} \int_0^h u \, dy = 0 \quad (4.19)$$

Substituting for  $u$  from (4.18) into (4.19) and integrating with respect to  $y$  gives,

$$h_t + J + \frac{1}{3} S(h_{xxx} h^3)_x = 0 \quad (4.20)$$

Equations (4.19) – (4.20) relate evaporative flux  $J$  with film thickness  $h(x, t)$ .

## 4.2 Expression for evaporation rate

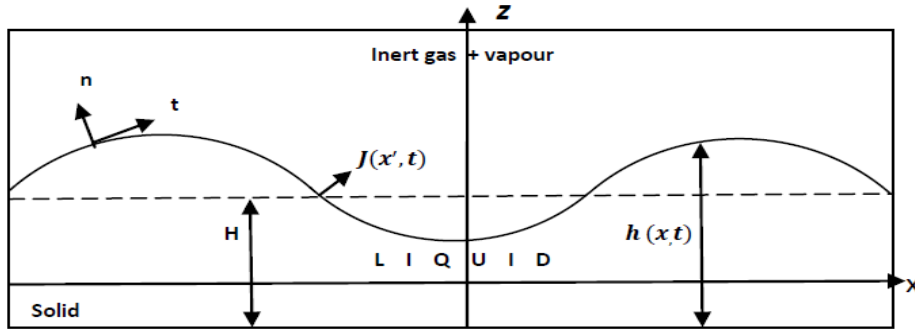


**Figure 17:** The air is not saturated with vapor. Concentration of vapor is function of  $x$ ,  $z$ , and  $t$ .

In chapter 2 and 3, it was assumed that film thickness was independent of the  $x$  – coordinate, but now a two dimensional system is considered and film thickness is no longer independent of  $x$ -coordinate i.e.  $h(x, t)$ . Concentration of vapor is function of space ( $x$ -coordinate and  $z$ -coordinate) and time i.e.  $c(x, z, t)$ . The gas phase is not saturated with vapor. Evaporation is limited by diffusion of vapor in the gas phase. Again, convective transport of water is ignored as in chapter 3 based on the assumption that gas phase speed is very small in controlled environments such as lab under at standard temperature ( $25^0C$ ) and pressure ( $1 atm$ ). Also, in section (4.1) lubrication model (4.19) was developed which involves evaporation rate  $J$ , therefore an analytical expression for the evaporation rate  $J$  is needed. This section deals with obtaining this expression.

The evaporation velocity of water vapor,  $10^{-9} ms^{-1}$ , is very small as compared to diffusion velocity,  $10^{-5} ms^{-1}$  under standard temperature and pressure (ref.4), hence quasi-static diffusion is considered i.e.  $\frac{\partial c}{\partial t} = 0$ . Thus, diffusion equation for two dimensional system is given by equation (4.22). In order to maintain condition of

non-saturation of vapor phase, a constant diffusion rate is assumed at  $z = +\infty$  (4.23). Since the film thickness is small, computed to its horizontal extent the position of the interface  $z = h'(x, t)$  is scaled by  $\epsilon h(x, t)$  where  $\epsilon = L_y/L_x$  and  $h(x, t) \sim 1$ . The vapor concentration  $c(x, \epsilon h(x, t), t)$  at the air-water interface now has dependency on the small parameter  $\epsilon$  where  $z = \epsilon h(x, t)$ . Since concentration of the water vapors in this mathematical problem exhibits dependence on the small parameter  $\epsilon$ , thus, according to perturbation theory, solution Taylor expanded in  $\epsilon$  is assumed for  $c(x, z)$  (4.21). Further, Non-dimensionalised concentration at the interface is given by equation (4.24)

$$c(x, t) = c_0 + \epsilon c_1 + \epsilon^2 c_2 + \epsilon^3 c_3 + \dots \quad (4.21)$$

Hence the PDE and the corresponding BC's are,

PDE

$$\frac{\partial^2 c}{\partial x^2} + \frac{\partial^2 c}{\partial z^2} = 0 \quad (4.22)$$

BC's

$$\frac{\partial c}{\partial z} (x, z = +\infty) = -1 \quad (4.23)$$

$$c(\epsilon h(x, t)) = 0 \quad (4.24)$$

Space variable  $z$  is scaled by  $h_0$ , vapor concentration is scaled through following equation.

$$c' = c_l' + \left(\frac{J_0 h_0}{D}\right) c$$

Where  $c_l'$  is the vapor concentration at the air-film interface.  $J_0$  is the characteristic evaporation rate specific to a liquid under reference conditions. Characteristic evaporation rate can be calculated from evaporation velocity ( $v_e$ ) specific to a particular liquid and density of that liquid ( $\rho_l$ ), ( $J_0 = \frac{v_e}{\rho_l}$ ).

Now, Taylor expanding  $c(x, z, t)$  about  $z = 0$ , substituting  $z = \epsilon h(x, t)$  and applying BC (4.24) led to,

$$0 = \sum_n \sum_m \epsilon^{n+m} \frac{h(x, t)^n}{n!} \frac{\partial^n c_m}{\partial z^n} (x, 0, t) \quad (4.25)$$

For convenience, from here onwards dependency on  $t$  will not be explicitly shown. Substituting perturbation expansion (4.21) for  $c$  in (4.25),

$$\begin{aligned} 0 = & c_0(x, 0) + \epsilon \left\{ c_1(x, 0) + h(x) \frac{\partial c_0}{\partial z} (x, 0) \right\} \\ & + \epsilon^2 \left\{ c_2(x, 0) + h(x) \frac{\partial c_1}{\partial z} (x, 0) + \frac{h(x)^2}{2} \frac{\partial^2 c_0}{\partial z^2} (x, 0) \right\} \\ & + \epsilon^3 \left\{ c_3(x, 0) + h(x) \frac{\partial c_2}{\partial z} (x, 0) + \frac{h(x)^2}{2} \frac{\partial^2 c_1}{\partial z^2} (x, 0) \right. \\ & \quad \left. + \frac{h(x)^3}{6} (x, 0) \right\} \\ & + O(\epsilon^4). \end{aligned} \quad (4.26)$$

Substituting equation (4.21) into BC (4.23) and matching powers of  $\epsilon^n$ ,

$$c_0 = -z,$$

Then, Equating each  $\epsilon^m$  terms in (4.26) to 0,

$$c_1(x, 0) = -h(x) \frac{\partial c_0}{\partial z} (x, 0) = f_1 \quad (4.27)$$

$$c_2(x, 0) = - \left[ h(x) \frac{\partial c_1}{\partial z} (x, 0) + \frac{h(x)^2}{2} \frac{\partial^2 c_0}{\partial z^2} (x, 0) \right] = f_2$$

$$c_3(x, 0) = - \left[ h(x) \frac{\partial c_2}{\partial z} (x, 0) + \frac{h(x)^2}{2} \frac{\partial^2 c_1}{\partial z^2} (x, 0) + \frac{h(x)^3}{6} \frac{\partial^3 c_0}{\partial z^3} (x, 0) \right] = f_3$$

$\frac{\partial^2 c_0}{\partial z^2}$  and  $\frac{\partial^3 c_0}{\partial z^3}$  are eliminated since  $c_0 = -z$ .

Taking Fourier transform of  $c_i(x, 0)$  in equation (4.27) with respect to  $x$ -space and using BC's (4.23-4.24) gives,

$$c_i(x, z) = \mathcal{F}^{-1}(\mathcal{F}[f_i] e^{-kz}) \quad (4.28)$$

Where,  $i = 1, 2$  and  $3$ .

$x$ -Fourier transform is used here to transform mathematical function of  $x$ -space  $f(x, z)$  into a new function  $F(k, z)$ . Any  $f(x, z)$  can be represented by summation of sinusoidal waves of different frequencies therefore Fourier transform generates a function  $F(k, z)$  in the  $k$  space which is the plot of amplitude of the real part of sinusoids and the imaginary part of the sinusoids as a function of  $k$ . The  $x$ -Fourier transform can be defined as

$$\mathcal{F}[f(x, z)](k) = F(k, z) = \frac{1}{2\pi} \int dx f(x, z) e^{-ikx}$$

$$\mathcal{F}^{-1}[F(k, z)] = f(x, z) = \frac{1}{2\pi} \int dk F(k, z) e^{ikx}$$

Taking  $x$ -Fourier transform of equation (4.22) gives  $C_n(k, z) = A(k)e^{-|k|z}$ .

Where  $C_n(k, z) = \mathcal{F}[c_n(x, z)](k)$  and taking  $x$ -Fourier transform of  $c_n(x, 0)$  in equation (4.27) gives  $A(k)$ . Hence, now taking inverse transform of  $C_n(k, z)$  gives  $c_n(x, z)$ . Here  $n = 1, 2, 3$  and  $\mathcal{F}^{-1}$  is the inverse Fourier transform.

Hilbert transform helps in converting  $c(x, 0)$  at the free boundary to  $\frac{\partial c}{\partial z}(x, 0)$  at the free boundary. This helps in determination of evaporation rate. In the present research thorough study on the properties of Hilbert transform was not done but, there was substantial use of the property,

$$\mathcal{F}^{-1}(|k|\mathcal{F}[f]) = -\frac{d}{dx}\mathcal{H}[f],$$

in order to obtain equation (4.25).

$$\begin{aligned} c_1(x, z) &= \mathcal{F}^{-1}(e^{-|k|z} \mathcal{F}[h]). \\ c_2(x, z) &= \mathcal{F}^{-1}\left(e^{-|k|z} \left(\mathcal{F}\left[-h \frac{d}{dx} \mathcal{H}[h]\right]\right)\right) \\ c_3(x, z) &= \mathcal{F}^{-1}\left(e^{-|k|z} \left(\mathcal{F}\left[h \left[-\frac{d}{dx} \mathcal{H}\left[-h \frac{d}{dx} \mathcal{H}[h]\right]\right]\right]\right)\right) \\ &\quad + \mathcal{F}^{-1}\left(e^{-|k|z} \left(\mathcal{F}\left[\frac{h^2}{2} h_{xx}\right]\right)\right) \end{aligned} \quad (4.29)$$

Thus, equation (4.29) gives the coefficients  $c_i(x, z)$  in the equation (4.21).

Hence solution for  $c(x, z)$  has been deduced which has dependence on film thickness  $h(x, t)$  up to  $O(\epsilon^3)$ .

Now, the evaporation rate  $J$  is given by

$$J = -\hat{n} \cdot \nabla c|_{z=\epsilon h} = -\frac{\partial z - \epsilon h_x \partial_x}{\sqrt{1 + \epsilon^2 h_x^2}} c(x, z)|_{z=\epsilon h} \quad (4.30)$$

$\sqrt{1 + \epsilon^2 h_x^2}$  is Taylor expanded to  $\left[1 - \frac{1}{2}(\epsilon^2 h_x^2) + O(\epsilon^4)\right]$ .  $h_x$  represents  $\frac{\partial h}{\partial x}$ .  $h(x, t)$  in the representation of  $\hat{n}$  is replaced by  $\epsilon h(x, t)$ ,  $\nabla c$  is the gradient of  $c$  and its dot product with unit normal vector,  $\hat{n}$  evaluated at point  $z = \epsilon h$ , gives the directional derivative i.e. rate of change of  $c(x, z)$  in the direction of unit normal vector  $\hat{n}$ . Then, equation (4.21) is substituted in place of  $c$  in the expression of  $J$ .

$$\begin{aligned} J = & \left[1 - \frac{\epsilon^2 h_x^2}{2} + O(\epsilon^4)\right] \left\{ -\frac{\partial c_0}{\partial z}(x, \epsilon h) \right. \\ & + \epsilon \left[ \frac{-\partial c_1}{\partial z}(x, \epsilon h) + h_x \frac{\partial c_0}{\partial x}(x, \epsilon h) \right] \\ & + \epsilon^2 \left[ \frac{-\partial c_2}{\partial z}(x, \epsilon h) + h_x \frac{\partial c_1}{\partial x}(x, \epsilon h) \right] \\ & + \epsilon^3 \left[ \frac{-\partial c_3}{\partial z}(x, \epsilon h) + h_x \frac{\partial c_2}{\partial x}(x, \epsilon h) \right] \\ & \left. + O(\epsilon^4) \right\} \quad (4.31) \end{aligned}$$

In (4.31),  $h_x \frac{\partial c_0}{\partial x}(x, \epsilon h) = 0$ , since  $c_0 = -z$ , Further each  $\frac{\partial c_n}{\partial z}$  term in (4.31) is Taylor expanded about  $z = 0$  corresponding to the order in  $\epsilon$ .  $n = 0, 1, 2, 3$ .

$$\begin{aligned}
J = & \left[ 1 - \frac{\epsilon^2 h_x^2}{2} + O(\epsilon^4) \right] \left\{ -\frac{\partial c_0}{\partial z} (x, 0) \right. \\
& + \epsilon \left[ -\frac{\partial c_1}{\partial z} (x, 0) - h \frac{\partial^2 c_0}{\partial z^2} (x, 0) \right] \\
& + \epsilon^2 \left[ -\frac{\partial c_2}{\partial z} (x, 0) - h \frac{\partial^2 c_1}{\partial z^2} (x, 0) - \frac{h^2}{2} \frac{\partial^3 c_0}{\partial z^3} \right. \\
& \left. + h_x \frac{\partial c_1}{\partial x} (x, 0) \right] \\
& + \epsilon^3 \left[ -\frac{\partial c_3}{\partial z} (x, 0) - h \frac{\partial^2 c_2}{\partial z^2} (x, 0) \right. \\
& - \frac{h^2}{2} \frac{\partial^3 c_1}{\partial z^3} (x, 0) - \frac{h^3}{6} \frac{\partial^4 c_0}{\partial z^4} (x, 0) \\
& \left. + h h_x \frac{\partial}{\partial z} \left( \frac{\partial c_1}{\partial x} \right) (x, 0) + h_x \frac{\partial c_2}{\partial x} (x, 0) \right] + o(\epsilon^4) \left. \right\} \tag{4.32}
\end{aligned}$$

Again,  $c_0 = -z$ , therefore the terms  $h \frac{\partial^2 c_0}{\partial z^2}$ ,  $\frac{h^2}{2} \frac{\partial^3 c_0}{\partial z^3}$ , and  $\frac{h^3}{6} \frac{\partial^4 c_0}{\partial z^4}$  in (4.32) are equal to 0.

Substituting  $c_i(x, z)$  from equation (4.29) into equation (4.32) and simplifying equation (4.32), gives

$$\begin{aligned}
J = & \left[ 1 + \epsilon \frac{d}{dx} \mathcal{H}[h] + \frac{\epsilon^2 h_x^2}{2} + \epsilon^2 \frac{d}{dx} \mathcal{H} \left[ h \frac{d}{dx} \mathcal{H}[h] \right] \right. \\
& - \frac{\epsilon^3 h_x^2}{2} \frac{d}{dx} \mathcal{H}[h] + h \epsilon^3 h_x \frac{d^2}{dx^2} \mathcal{H}[h] \\
& - \epsilon^3 \frac{d}{dx} \mathcal{H} \left[ h \left[ \frac{d}{dx} \mathcal{H} \left[ h \frac{d}{dx} \mathcal{H}[h] \right] \right] \right] \\
& - \epsilon^3 \frac{d}{dx} \mathcal{H} \left[ \frac{h^2}{2} h_{xx} \right] + \epsilon^2 h \frac{d^2 h}{dx^2} \\
& - \epsilon^3 h \frac{d^2}{dx^2} \left[ h \frac{d}{dx} \mathcal{H}[h] \right] \\
& + \epsilon^3 \frac{h^2}{2} \frac{d^3}{dx^3} \mathcal{H}[h] - \epsilon^3 h_x \frac{d}{dx} \left[ h \frac{d}{dx} \mathcal{H}[h] \right] \\
& \left. + O(\epsilon^4) \right] \tag{4.33}
\end{aligned}$$

Equation (4.33) is the complete expression for the evaporation rate  $J$ . Sultan et al. <sup>[4]</sup> chose to set the  $\epsilon^n = 1$  in the expression for evaporation rate provided in their research paper, which is not correct because using the assumption of  $\epsilon$  being small in order to scale  $y' = h'(x', t')$  and then setting  $\epsilon = 1$  later on is not a valid mathematical approach.

Also, the equation for  $J$  provided by Sultan et al. has incorrect addition and subtraction signs for some terms, incorrect terms and is also missing  $-\epsilon^3 \frac{h^2}{2} \frac{d^3}{dx^3} \mathcal{H}[h]$  and  $\epsilon^3 h_x \frac{d}{dx} \left[ h \frac{d}{dx} \mathcal{H}[h] \right]$  terms which has been added in the expression for evaporation rate above. Terms highlighted in red color in (4.33) indicate incorrect signs and/or incorrect terms. Terms highlighted in blue in (4.33) indicate missing terms.

Hence equation (4.33) is the complete and newer version of the expression of evaporation rate  $J$  for the wrinkled air-water interface.

The expression for evaporation rate  $J$  can now be substituted in to the lubrication model (4.19) thus, we have complete model that relates film thickness with evaporation rate and fluid motion. Using robust computational software, analytical solution for the evolution of film thickness using the lubrication model can now be obtained.

## Chapter 5

### CONCLUSIONS

The aim of the research was to model the evaporation of the tear film of the eye, which is the major cause of Evaporative DES of the eye, using mathematical models. Evaporation is regarded as diffusion limited process in development of these models.

In chapter 2, research work done by Ajaev et al. 2010 on the evaporation of the thin film was referred to. The partial differential equations were developed under the assumption of negligible film thickness compared to the domain size of vapor diffusion, negligible fluid motion and flat interface. Concept of equal vapor and liquid chemical potential and London van-der Waals model for conjoining pressure was used to provide an equation for the concentration of the vapor at the air-water interface. These equations provided a good starting point for numerical simulation of evolution of film thickness and concentration profile across the domain as a function of time. The results in chapter 2 indicate that film thickness did approach an equilibrium value fast i.e. evaporation is suppressed early and the mass lost from the liquid diffuses along the z-coordinate. Nevertheless, steady state concentration at different values in the z-coordinate was reached after a long time and was equal to relative humidity chosen. This matched the theoretical prediction that steady state concentration should be equal to relative humidity of the atmosphere.

In chapter 3, assumption of negligible thickness was relaxed, thus a new variable had to be introduced to scale the moving domain into fixed domain which

resulted in modified PDE's, BC's and IC's. Numerical simulation demonstrated the effect of the length of the domain of diffusion on the concentration profile across the domain and it was concluded that having a desiccant (constant far field concentration) near the film decreased the time to reach steady state concentration across the domain. Also, the concentration profile and film thickness evolution for the moving domain problem were indeed different than the ones presented in chapter 2 where negligible thickness assumption was used in the simulation. The film thickness in the moving boundary problem approached equilibrium value slower than the film thickness in the fixed boundary problem (chapter 2). Concentration profile for fixed and moving domain also followed different trends compared to each other. Hence, solution to moving boundary problem provided a more accurate description for the evaporation of the thin film.

In chapter 4, fluid motion and wrinkled air-water interface were taken into account and expression for evaporation rate provided by Sultan et al. 2004 was derived again. First, Lubrication model was developed by non-dimensionalizing Navier-Stokes equations and using the equations for boundary stresses. The derived Lubrication model gave relation between fluid motion, film thickness and evaporation rate. Later, expression for the evaporation rate was deduced by solving the two-dimensional quasi steady state diffusion problem with constant diffusion rate at infinity in the z-coordinate. This expression of evaporation rate was then compared with the one provided by Sultan et al. and it was found that the expression provided by Sultan et al. was missing epsilon,  $\epsilon$  as well as was missing certain terms. Thus, a newer accurate version of evaporation rate has been provided in the chapter 4.

## REFERENCES

1. Braun, Richard J. "Dynamics of Tear Film." *Annual Review of Fluid Mechanics* 44 (2012): 267-97.
2. King-Smith, P. E., Nichols, J. J., Nichols, K. K., Fink, B. A., and Braun, R. J. "Contributions of Evaporation and Other Mechanisms to Tear Film Thinning and Break-up." *Optometry and Vision Science*, (2008); 85.8: 623-36.
3. Ajaev, V. S., Brutin, D., and Tadrist, L. "Evaporation of Ultra-thin Liquid Films into Air." *Microgravity Sci.Technol.* (2010); 22: 441-446.
4. Sultan, E., Boudaoud, A., and Amar, M. B. "Diffusion-limited evaporation of thin polar liquid films." *Journal of Engineering Mathematics* (2004); 50: 209-222.
5. Ehlers N. 1965. The precorneal film: biomicroscopical, histological and chemical investigations. *Acta Ophthalmol. Suppl.* 81:1–134
6. Mishima S. Some physiological aspects of the precorneal tear film. *Arch. Ophthalmol.* 1965; 73:233–41
7. McCulley J. .P, and Shine, W. A compositional based model for the tear film lipid layer. *Trans. Am. Ophthalmol. Soc.* 1997; 95:79–93
8. Bron, A. J., Tiffany, J. M., Gouveia, S. M., Yokoi, N., and Voon, L. W. Functional aspects of the tear film lipid layer. *Exp. Eye Res.* 2004; 78:347–60
9. Holly, F. J. Formation and rupture of the tear film. *Exp. Eye Res.* 1973; 15:515-25.
10. Nichols, J. J., Mitchell, G. L., and King-Smith, P. E. Thinning rate of the pre-corneal and prelens tear films. *Invest Ophthalmol Vis Sci* 2005; 46: 2353-61.
11. Levin, M. H., and Verkman, A. S. Aquaporin-dependent water permeation at the mouse ocular surface: in vivo microfluorimetric measurements in cornea and conjunctiva. *Invest Ophthalmol Vis Sci* 2004; 45: 4423-32.
12. G.Bharathi, and I.Gipson. "Membrane-tethered mucins have multiple functions on the ocular surface." *Experimental Eye Research.* 90.2010 (2010): n. page. Print.

13. Abelson, Mark, Darlene Dartt, et al. "Mucins: Foundation of A Good Tear Film." *Review of Ophthalmology*. (2011): n. page. Print.  
<[http://www.revophth.com/content/d/therapeutic\\_topics/c/30968/](http://www.revophth.com/content/d/therapeutic_topics/c/30968/)>.
14. Vladimir, Ajaev. *Interfacial Fluid Mechanics: A Mathematical Modeling Approach*. Springer, 2012. Print.
15. Van der Waals Interactions – Hamaker Constant.  
<http://chemeng.queensu.ca/courses/CHEE460/lectures/documents/CHEE4602010Lecture5.pdf>. Assessed on 03/31/2013.
16. Barash, L. Yu, Bigioni, T. P., Vinokur, V. M., and Shchur, L. N. Evaporation and fluid dynamics of a sessile drop of capillary size. *Phys. Rev. E*. 2009; 79:046301.1-16.
17. Deegan, R.D., Bakajin, O., Dupont, T. F., Huber, G., Nagel, S. R., and Witten, T. A. Contact line deposits in an evaporating drop. *Phys. Rev. E*. 2000; 62:756-765.
18. Online Calculators." *Holsoft's Physics Resources Pages*. N.p., n.d. Web.  
<<http://www.holsoft.nl/physics/ocmain.htm>>.

## Chapter 6

### APPENDIX

#### 6.1 Code used for numerical simulation (Ch-2 and Ch-3)

```
function [t, f] = test4UpDate(nx,t_f,Lf,W)

% By Vikramjit Singh Rathee and Dr. Richard Braun.

% -----
% -----

% THIS IS UPDATED AND NEW TEST CODE. SO test.m AND test2.m WON'T BE
NEEDED NOW

% test3.m IS JUST A TEST CODE FOR TESTING FIXED CONDITION UNDER TWO
% DIFFERENT CIRCUMSTANCES ( ZETA = Z/L AND JUST Z)

% THIS CODE PRODUCES ALL THE PLOTS OF evap.m AND evap2.m, HENCE THESE
CODES
% WON'T BE NEEDED ANYMORE.

% H is changed to C_H for convenience

% THK is abbreviation for thickness

close all

% This is for moving boundary problem
% nx is the spacing

% Initialization

h0 = 1; % refer to figure in Ajaev
ep = 0.001; % given in ajaev figure
```

```

    C_H = 1/4 * exp( - ep / h0^3 ); % constant far field
concentration (1/4 the initial conc. at interface), a constant number
= 0.2498
    h_inf = (-ep/log(C_H))^(1/3); % equilibrium thickness
% total nx+1 grid points for nx spacing
    dx = 1 / (nx+1);
    tspan = [0 t_f]; % giving time span with time steps.

% Concentration is non-dimensionalised.

%Initial Conditions
    f0 = ones(nx + 1, 1);
    f0(1) = h0; % Initial height of the film.
    c0 = exp( -ep / h0^3 );
    for i = [2:(nx+1)]
        f0(i) = (c0-C_H)*exp((-i*dx)/0.05)+C_H;
        % conc. at all grid points (except z=0) at t=0.
        % exp function so as to make smooth curve of intial points
with
        % i*dx, so that intial condition does not drop from c0 to C_H
        % directly making it not smooth.
    end

% System of ODES FOR MOVING CONDITION
function dt_f = fdot(t,f)

    h = f(1);
    c = f(2:end);
    dt_c = zeros(nx,1);
    dt_f = zeros(nx+1,1); %Output of this function; 1 column.

    c0 = exp( -ep / h^3 ); % conc. at the interface., model for
conjoining pressure
                                % due to which equilibrium thickness
is
                                % reached
    cf = C_H; % which is a constant value.

% ODE for h & c using central difference formula

    dt_h = 1/(Lf-h)*(-c(2)+4*c(1)-3*c0)/(2*dx);

% Finite Differences discretized space, c
% Boundary, c

```

```

        dt_c(1) = 1/(Lf-h)^2 * ( c(2) - 2* c(1) + c0 ) / dx^2 -
        ((c(2)-c0)/(2*dx)) * ((-c(2)+4*c(1)-3*c0)/(2*dx)) * ((1*dx)-1)/(Lf-
h)^2);
        dt_c(nx) = 1/(Lf-h)^2 * ( cf - 2*c(nx) + c(nx-1) ) / dx^2 -
        ((cf-c(nx-1))/(2*dx)) * ((-c(2)+4*c(1)-3*c0)/(2*dx)) * ((nx*dx)-
1)/(Lf-h)^2);

        % Middle, c
        for i = [2:(nx-1)]
            dt_c(i) = 1/(Lf-h)^2 * ( c(i+1) - 2*c(i) + c(i-1) ) /
dx^2 - ((c(i+1)-c(i-1))/(2*dx)) * ((-c(2)+4*c(1)-
3*c0)/(2*dx)) * ((i*dx)-1)/(Lf-h)^2);
        end

        dt_f = [dt_h;dt_c]; % 1st row (1st grid) is the ODE for h and
rest rows (grids) are ODE's for conc.
        end

% SOLVING ODE for MOVING condition
myTol = odeset('RelTol',1e-5,'AbsTol',1e-6);
[t2,f] = ode45(@fdot, tspan, f0,myTol);
[t_moving,f_moving] = ode45(@fdot, [0 1 t_f/20 t_f/4 t_f/2 t_f],
f0,myTol);
h_moving = f(:,1);

if W == 0 || W == 3

% PLOT OF CONC. MOVING
% "discrete" takes into account only the conc. values at specified
time points
c0 = exp( -ep ./ f(:,1).^3 );
c0_discrete_moving = exp( -ep ./ f_moving(:,1).^3 );
cf = C_H*ones(size(c0)); % a column vector of 0.2498 of size c0.
cf_discrete_moving = C_H*ones(size(c0_discrete_moving));
f_a_moving = [c0,f(:,2:end),cf]; % Matrix of concentrations, each
column for different grid point and each row for different time
f_a_moving_discrete =
[c0_discrete_moving,f_moving(:,2:end),cf_discrete_moving];

% CREATING a distance positioning vector from 0 to 1, i.e. zeta
% new coordinate system 0<zeta<1, see linspace command.
X = linspace(0,1,length(f0)+1);
% +1 cause need coordinate for cf too

```

```

    % condensing all the grid points between 0 and 1.

z_new = linspace(0,Lf,length(f0)+1);

% Z coordinates at different t dependent upon zeta and h(t)
Z_moving_0 = (X*(Lf-f_moving(1,1)))+ f_moving(1,1);
Z_moving_one = (X*(Lf-f_moving(2,1)))+ f_moving(2,1);
Z_moving_twenty = (X*(Lf-f_moving(3,1)))+ f_moving(3,1);
Z_moving_fourth = (X*(Lf-f_moving(4,1)))+ f_moving(4,1);
Z_moving_half = (X*(Lf-f_moving(5,1)))+ f_moving(5,1);
Z_moving_end = (X*(Lf-f_moving(6,1)))+ f_moving(6,1);

% Plot of CONC. VS ZETA for different TIMES
figure
plot(X,f_a_moving_discrete(2,:), 'g-', 'Linewidth',2);
hold on
plot(X,f_a_moving_discrete(3,:), 'b-', 'Linewidth',2);
hold on
plot(X,f_a_moving_discrete(4,:), 'k-', 'Linewidth',2);
hold on
plot(X,f_a_moving_discrete(5,:), 'c-', 'Linewidth',2);
hold on
plot(X,f_a_moving_discrete(6,:), 'm-', 'Linewidth',2);
hold off
legend( sprintf('time = %4.2f', t_f/20), 'time = 10', sprintf('time = %4.2f', t_f/4), sprintf('time = %4.2f', t_f/2), sprintf('time = %4.2f', t_f))
xlim([0 1])
xlabel('$\zeta$', 'Interpreter', 'latex', 'FontSize',12)
ylabel('c($\zeta$,t)', 'Interpreter', 'latex', 'FontSize',12)
end

if W == 0
% Plot of h(t)-h(infty)
figure
semilogy(t2,abs(f(:,1)-h_inf))
xlabel('time t', 'Interpreter', 'latex', 'FontSize',12)
ylabel('h-h$\infty$', 'Interpreter', 'latex', 'FontSize',12)
end

if W == 0
% 3D plot MOVING
figure

waterfall(z_new',t2,f_a_moving)

%     xlabel('$\zeta$', 'Interpreter', 'latex', 'FontSize',12)
%     ylabel('t')
%     zlabel('c($\zeta$,t)', 'Interpreter', 'latex', 'FontSize',12)

```

```

        xlabel('z','Interpreter','latex','FontSize',12)
        ylabel('t')
        zlabel('c(z,t)','Interpreter','latex','FontSize',12)
    end

%FIXED CONDITION

% System of ODES for FIXED

function dt_f2 = fdot2(t,f)
    % Initialization
    dt_f2 = zeros(nx+1,1);
    c0 = exp( -ep / f(1)^3 ); % conc. at the interface.
    cf = C_H; % which is a constant value.

    % Forward Difference, h

    dt_f2(1) = 1/(Lf)*(-f(3)+4*f(2)-3*c0)/(2*dx);

    % Finite Differences discretized space, c
    % Boundary, c
    dt_f2(2) = (1/(Lf^2))*( f(3) - 2* f(2) + c0 ) / dx^2;
    dt_f2(nx+1) = (1/(Lf^2))*( cf - 2*f(nx+1) + f(nx) ) / dx^2;

    % Middle, c
    for i = [3:(nx)]
        dt_f2(i) = (1/(Lf^2))*( f(i+1) - 2*f(i) + f(i-1) ) /
dx^2;
    end
end
end

```

```

% Solve ODE for FIXED
[t1,f] = ode45(@fdot2, tspan, f0,myTol);
[t_fixed,f_fixed] = ode45(@fdot2, [0 1 t_f/20 t_f/4 t_f/2 t_f],
f0,myTol);
analytical = 1 + 2 / sqrt(pi) * ( C_H-1)*sqrt(t1);
h_fixed = f(:,1);

if W == 0 || W == 1
% Creating CONC. Matrix

c0 = exp( -ep ./ f(:,1).^3 );
c0_discrete_fixed = exp( -ep ./ (f_fixed(:,1)).^3 ); % contains
c0 at fixed time points

cf = C_H*ones(size(c0)); % a column vector of 0.2498 of size c0.
cf_discrete_fixed = C_H*ones(size(c0_discrete_fixed));

f_a_fixed = [c0,f(:,2:end),cf]; % Matrix of concentrations, each
column for different grid point and each row for different time
f_a_fixed_discrete = [c0_discrete_fixed, f_fixed(:,2:end),
cf_discrete_fixed]; % this makes sure that at end point conc. at all
times

% regardless of the Lf is H

% Creating Z-Coordinate
X_fixed = linspace(0,1,length(f0)+1); % +1 cause need coordinate for
cf too
X_new = Lf.*X_fixed;

% CONC. plot at end time
figure
plot(X_new,f_a_fixed(end,:), 'b-', 'Linewidth',2)
xlabel('z', 'Interpreter', 'latex', 'FontSize',12)
ylabel('c(z,t)', 'Interpreter', 'latex', 'FontSize',12)
title(sprintf('time = %d', t_f))

end

if W == 1
% 3D Plot
figure
waterfall(X_new',t1,f_a_fixed)
xlabel('z', 'Interpreter', 'latex', 'FontSize',12)

```

```

        ylabel('t')
        zlabel('c(z,t)', 'Interpreter', 'latex', 'FontSize', 12)
end

```

```

if W == 0 || W == 1
% For plotting c(z,t) vs. z comparison for Moving and Fixed boundary
figure

subplot(3,2,1),plot(X_new,f_a_fixed_discrete(1,:), 'r', Z_moving_0, f_a_
moving_discrete(1,:), 'b-', [f_moving(1,1) f_moving(1,1)], [0 1], 'k--
', [0 Lf], [C_H C_H], '--g', 'Linewidth', 2)
    xlabel('z', 'Interpreter', 'latex', 'FontSize', 12)
    ylabel('c(z,t)', 'Interpreter', 'latex', 'FontSize', 12)
    title(sprintf('time = 0 and L = %g', Lf))
    legend('Domain 0 to L', 'Domain h to L', 'Tear film THK', 'Relative
humidity', 'location', 'best')

subplot(3,2,2),plot(X_new,f_a_fixed_discrete(2,:), 'r', Z_moving_one, f_
a_moving_discrete(2,:), 'b-', [f_moving(2,1) f_moving(2,1)], [0 1], 'k--
', [0 Lf], [C_H C_H], '--g', 'Linewidth', 2)
    xlabel('z', 'Interpreter', 'latex', 'FontSize', 12)
    ylabel('c(z,t)', 'Interpreter', 'latex', 'FontSize', 12)
    title(sprintf('time = %d', 1))

subplot(3,2,3),plot(X_new,f_a_fixed_discrete(3,:), 'r', Z_moving_twenty
, f_a_moving_discrete(3,:), 'b-', [f_moving(3,1) f_moving(3,1)], [0
1], 'k--', [0 Lf], [C_H C_H], '--g', 'Linewidth', 2)
    xlabel('z', 'Interpreter', 'latex', 'FontSize', 12)
    ylabel('c(z,t)', 'Interpreter', 'latex', 'FontSize', 12)
    title(sprintf('time = %4.2f', t_f/20))

subplot(3,2,4),plot(X_new,f_a_fixed_discrete(4,:), 'r', Z_moving_fourth

```

```

,f_a_moving_discrete(4,:), 'b-', [f_moving(4,1) f_moving(4,1)], [0
0.8], 'k--', [0 Lf], [C_H C_H], '--g', 'Linewidth',2)
xlabel('z', 'Interpreter', 'latex', 'FontSize',12)
ylabel('c(z,t)', 'Interpreter', 'latex', 'FontSize',12)
title(sprintf('time = %4.2f', t_f/4))

subplot(3,2,5),plot(X_new,f_a_fixed_discrete(5,:), 'r', Z_moving_half,f_
_a_moving_discrete(5,:), 'b-', [f_moving(5,1) f_moving(5,1)], [0
0.4], 'k--', [0 Lf], [C_H C_H], '--g', 'Linewidth',2)
xlabel('z', 'Interpreter', 'latex', 'FontSize',12)
ylabel('c(z,t)', 'Interpreter', 'latex', 'FontSize',12)
title(sprintf('time = %d', t_f/2))

subplot(3,2,6),plot(X_new,f_a_fixed_discrete(6,:), 'r', Z_moving_end,f_
_a_moving_discrete(6,:), 'b-', [f_moving(6,1) f_moving(6,1)], [0 0.4], 'k-
-', [0 Lf], [C_H C_H], '--g', 'Linewidth',2)
xlabel('z', 'Interpreter', 'latex', 'FontSize',12)
ylabel('c(z,t)', 'Interpreter', 'latex', 'FontSize',12)
title(sprintf('time = %d', t_f))

% For plotting thickness of the film
figure
plot(t1, h_fixed,t2, h_moving,t1, analytical, 'Linewidth',2)
ylim([0 1])
xlim([0 10])
legend('numerical solution (fixed boundary)', 'numerical solution
(moving boundary)', 'analytical solution w/o conjoining pressure, \Pi
= 0', 'location', 'best')
xlabel('time t', 'Interpreter', 'latex', 'FontSize',12)
ylabel('Thickness of the film
h', 'Interpreter', 'latex', 'FontSize',12')
title(sprintf('L = %d', Lf))

figure
plot(t1, h_fixed,t1, analytical, 'Linewidth',2)
ylim([0 1])
xlim([0 10])
legend('numerical solution (fixed boundary)', 'analytical solution
w/o conjoining pressure, \Pi = 0', 'location', 'best')
xlabel('time t', 'Interpreter', 'latex', 'FontSize',12)
ylabel('Thickness of the film
h', 'Interpreter', 'latex', 'FontSize',12')
title(sprintf('L = %d', Lf))

end
end

```

